Effect of senescence on biogenic volatile organic compound fluxes in wheat plants

Lais Gonzaga Gomez, Benjamin Loubet, Florence Lafouge, Raluca Ciuraru, Sandy Bsaibes, Julien Kammer, Pauline Buysse, Brigitte Durand, Jean-Christophe Gueudet, Olivier Fanucci, et al.

Effect of senescence on biogenic volatile organic compound fluxes in wheat plants

Lais Gonzaga Gomez[1], Benjamin Loubet[1], Florence Lafouge[1], Raluca Ciuraru[1], Sandy Bsaibes[3], Julien Kammer[1,2], Pauline Buysse[1], Brigitte Durand[1], Jean-Christophe Gueudet[1], Olivier Fanucci[1], Olivier Zurfluh[1], Céline Decuq[1], François Truong[3], Valérie Gros[3] and Christophe Boissard[3,4].

(1) UMR ECOSYS, INRAE, AgroParisTech, Université Paris-Saclay, 78850, Thiverval-Grignon, France.
(2) now at Department of Chemistry and Environmental Research Institute, University College Cork, Cork, Ireland.
(3) LSCE, CNRS-CEA-UVSQ, IPSL, 91 191, Gif sur Yvette, France.
(4) Université de Paris, and UPEC, CNRS, LISA, 94000 Créteil, France.

Corresponding author: benjamin.loubet@inrae.fr

Abstract. Exchanges of biogenic volatile organic compounds (BVOC) between plants and the atmosphere are likely to vary, in amount and composition, between different plant species but also for a single plant during its development. However, the effect of plant development stages, including senescence, on BVOC exchanges remains poorly investigated, especially in the case of crop plants. We investigated the BVOC exchange patterns for wheat plants, the most grown crop species worldwide, during seed maturation, senescence and after harvest. Fluxes were measured online, *in situ*, at the plant scale by combining automated chambers and a Proton Transfer - Reaction - Quadrupole ion guide - Time of Flight - Mass Spectrometer (PTR-Qi-Tof-MS). The high resolution and sensitivity of this method enabled the measurement of a large mass spectrum of compounds emitted at very small amounts, allowing a precise characterization of BVOC exchanges. We found that the overall BVOC emissions increased twofold during the senescence stage compared to the maturation stage. Methanol was found to be the most emitted compound (49 – 60% of the overall flux on a molar basis) followed by acetone (7.5 – 8.2% of the overall flux on a molar basis) during each developmental stage investigated. Acetaldehyde was another

major emitted compound contributing mainly during late senescence to the overall flux (9.7%). When normalized for temperature and light conditions, most BVOC emissions increased during senescence, showing a clear effect of senescence on BVOC exchanges. Chamber emissions were comparable to whole ecosystem fluxes measured at the same site by eddy covariance the previous year. The OH reactivity of the emitted compounds was evaluated based on known reaction rate constants and was the largest during the first senescence stage, peaking at 12 s^{-1} in the chambers. The results of this study show the need for considering plant phenology when computing BVOC emissions from crops.

Keywords: BVOC, dynamic chamber, crop, development stage, PTR-Qi-Tof-MS.

1. Introduction

Plants synthesize and release an incredible diversity of volatile organic compounds (VOCs) into the atmosphere; more than 1700 biogenic VOCs (BVOCs) have already been identified (Knudsen et al. 2006). BVOC emissions from terrestrial vegetation are estimated to be 760 Tg (C) yr^{-1} representing 90% of total emissions at global scale (Sindelarova et al., 2014). Besides the importance of these compounds in the interaction between plants and their environment, BVOCs are known to impact air quality, climate, human health and vegetation. Indeed BVOCs contribute to the formation of tropospheric ozone (Fehsenfeld et al., 1992), of secondary organic aerosols (SOA) (Ziemann and Atkinson, 2012) and increase the lifetime of methane in the atmosphere by reducing the oxidative capacity of the atmosphere (Isaksen et al., 2009). These issues explain the growing interest, over the last decades, in BVOC emissions into the atmosphere.

BVOC species are diverse and include several organic classes such as terpenes, fatty acid derivatives, alcohols, alkanes, alkenes, esters and acids, among others (Pichersky and Gershenzon

2002; Peñuelas and Llusià 2001). Several factors influence - quantitatively and qualitatively - BVOC exchanges between plants and the atmosphere. First, the biosynthesis of VOCs by plants is strongly linked to the genetic information of the plant (Degen et al. 2004; Delphia et al. 2009; Splivallo et al. 2012). Thus, emissions of these compounds vary greatly from one species to another and even within the same plant species (Gonzaga Gomez et al., 2019; Splivallo et al., 2012). Secondly, BVOC exchanges depend also on environmental factors, such as temperature, light, relative humidity, atmospheric CO_2 and O_3 concentrations, nutrient availability and soil moisture (Gouinguené and Turlings, 2002; Laothawornkitkul et al., 2009; Staudt and Bertin, 1998). Finally, it has been shown that BVOC exchanges depend also on specific characteristics of the plant, varying for example during plant development (Bachy, 2018; Bracho-Nunez et al., 2011; Mozaffar et al., 2018; Rottenberger et al., 2005).

BVOC exchanges during different developmental plant stages have so far been poorly investigated. In addition, most of the existing studies have focused mainly on the developmental effect on isoprenoids and methanol emissions. For example, it has been reported that methanol emissions are strongly associated with plant growth (Bracho-Nunez et al., 2011). Indeed, this compound is formed in plants from the demethylation of pectin, a mechanism occurring during cell wall alteration (Fall and Benson, 1996). An increase in emissions of this compound has also been observed during leaf senescence of maize plants (Mozaffar et al., 2018). It has also been shown that isoprene emission is lower in young leaves than in mature leaves. This may be due to a higher respiration rate competing for pyruvate, a common substrate to isoprene biosynthesis and respiratory processes (Loreto et al., 2007). Other examples are monoterpenes, sesquiterpenes and acetone showing higher emission rates in young leaves and reduced or non-existent emissions rates at leaf maturity (Bracho-Nunez et al., 2011).

It has been estimated that agricultural crops in Europe account for 27% of the overall BVOC emissions (Karl et al., 2009), which represents a non-negligible contribution. Despite the species-specific dependence of BVOC emissions, as mentioned before, most studies have focused on BVOC fluxes from trees and thus on isoprenoids. For this reason fluxes from agricultural plant species, which appear to be dominated by oxygenated VOCs (Karl, 2009), remain poorly understood. These estimates are in fact mostly based on measurements made on a few plant species, over a short time period and with analytical constraints. Therefore, since these measurements may not be representative of the variety of crops, and regions, the contribution of these ecosystems to the overall BVOC emissions remains inaccurate.

The widely used MEGAN 2.1 model (Guenther et al., 2012) provides estimates of BVOC emissions from terrestrial ecosystems. Despite the recent improvement of this model, the estimated emission rates from crops remain inaccurate (Guenther et al., 2012). This is mainly due to the assignment of emission factors by default to all crop species given the lack of emission rate measurements on these species. Indeed in MEGAN 2.1 crop plant species are all grouped into one “functional plant type” for which one emission factor value is attributed. Current knowledge, however shows that BVOC emissions vary strongly (composition and amounts) between species and even between varieties of the same species (Gonzaga Gomez et al., 2019). Thus, emission factors should be better investigated on most grown crop species such as wheat, rice, maize or oilseed rape. In addition, despite the dependence of VOC emissions on the plant's age, in the MEGAN 2.1 model, the plant developmental stage is not taken into account when estimating emissions for all oxygenated compounds, apart from methanol. In order to achieve a more reliable estimate of these emissions, more accurate emission factors for individual crop plants are

93 needed, as well as a better understanding of how the different drivers (e.g. light, temperature,
94 age) influence BVOC exchanges.

95 Wheat is the most widely grown crop in the world and in Europe, representing more than 15 %
96 and 33 % (FAOSTATS 2017) of the total croplands cultivated surface, respectively. However,
97 the studies on BVOC emissions from wheat plants are quite limited and show a large divergence
98 between results (Bachy, 2018; Butter et al., 1985; Gallagher et al., 2000; König et al., 1995;
99 Morrison et al., 2016; Piesik et al., 2011; Winer et al., 1992). Recently, Bachy (2018) conducted
100 a study over a wheat field where BVOC exchanges were investigated during the whole growing
101 season at the ecosystem level. The authors found that, like for most crop species, methanol was
102 the most emitted compound and the emissions of this compound and acetaldehyde increased with
103 plant senescence. However, their study could not distinguish between emissions originating from
104 plants and from soil. In addition, flux measurements were limited to a small number of
105 compounds in order to maintain a high measurement frequency, which raises questions of other
106 VOCs that could have been overlooked.

107 In order to improve the understanding and the quantification of BVOC fluxes in wheat crops, this
108 study aims to – (a) characterize, quantitatively and qualitatively, BVOC exchanges of wheat at
109 the plant level during ripening, senescence and harvest, over a wide spectrum of compounds; (b)
110 propose physiological mechanisms explaining the variations of emissions during the investigated
111 developmental stages and discuss how climatic factors (humidity, temperature, and light) can
112 influence these emissions. To achieve these objectives a Proton Transfer - Reaction - Quadrupole
113 ion guide - Time of Flight - Mass Spectrometer (PTR-Qi-Tof-MS) was used in combination with
114 multiple dynamic automated chambers for online measurements of BVOC fluxes from wheat

115 plants. The chamber fluxes were challenged against eddy covariance fluxes measured in a nearby
116 field the year before to verify the general relevance of our results.

117 2. Materials and methods

118 2.1. Site

119 Flux measurements took place on a field belonging to the experimental farm of Grignon owned
120 by AgroParisTech and located about 30 km west of Paris in France (48°51'N, 1°58'E). The site is
121 a 2 ha field, with a crop rotation of wheat and maize since 2011, located next to the ICOS FR-Gri
122 site on the south-east. The details about the ICOS site can be found in Loubet et al. (2011), Laufs
123 et al. (2017) or Vuolo et al. (2017).

124 Wheat (*Triticum aestivum L.*; Fructidor variety) was sown on October 21st, 2016 and harvested
125 on June 30th, 2017. Certain agricultural practices such as fertilizer, fungicide and herbicide
126 application are detailed in Appendix A. Indeed these practices are likely to impact the emissions
127 of VOC by plants as well as the measurements of these compounds.

128 2.2. Experimental campaign

129 The measurement campaign covered the period from June 10th to July 04th, 2017. Measurements
130 were performed simultaneously on two wheat plant replicates using two automated dynamic
131 chambers, based on the original design of Pape et al. (2009), modified and detailed in Gonzaga
132 Gomez et al. (2019). The complete plant above ground was enclosed in the ≈ 35 L chamber
133 placed outdoors in the field. In short, the chambers consisted of an acrylic glass (PMMA)
134 cylinder covered by a fully light-permeable FEP film (50 μm thick PTFE, MICEL). A motorized
135 lid also covered by FEP film was used to open the chambers between measurements intervals. A
136 quantum sensor (SOLEMS, PAR/CBE 80, Palaiseau, France) and a copper-constantan

thermocouple device ensured the continuous monitoring of air temperature and Photosynthetically Active Radiation (PAR) inside the chambers. An axial fan (D341T-012GK-2, MICRONEL) was used to purge ambient air into the cuvette at ≈ 14 L min^{-1}. Each chamber was equipped with two twenty-meter-long PFA sampling tubes (1/8 inch internal diameter): one for the inlet air (ambient air) and one for the outlet air (inside chamber air) sampling. Each of these sample tubes was heated to 50°C to avoid condensation of the air until it reached the PTR-Qi-ToF-MS (Ionicon, Analytik GmbH, AU), which was used to measure BVOC concentration at 10 Hz. In the present work, the instrument was operated at drift tube pressure and temperature of 4 ± 0.0001 mbar and 80 ± 0.06°C, respectively. The inlet flow rate was set to 150 ± 5.42 ml min^{-1} and the *E/N* value (where E is the electric field strength and N the gas density) to about 132 ± 0.03 Td (1 townsend = 10^{-17} V cm^2). An infrared gas analyzer (Li-Cor 840 model, Li-Cor, Lincoln, Nebraska, USA) was used to follow CO_2 and H_2O concentrations from the inlet and outlet air sampling of each chamber. In order to determine the effect of chambers on VOC measurements we previously measured on an empty chamber. We thus detected some heavy compounds emitted by the chambers (*m/z* 118.063, 190.962 and 192.960) which were removed from the analysis. Further details about the experimental device, including chambers and PTR-Qi-TOF-MS operation, can be found in Gonzaga Gomez et al. (2019).

2.3. PTR-MS concentration

The pre-processing steps provided averages and standard deviations of count rates (cps in counts per seconds) for the compounds (ion peaks) selected R_i. The mixing ratio of the compound χ_i(in ppbv) was calculated as in Abis et al., (2018) and Gonzaga Gomez et al. (2019):

$$\chi_i = 1.657\ 10^{-11} \times \frac{U_{drift}\ T_{drift}^2}{k\ p_{drift}^2} \times \left(\frac{cps^{norm}_{R_iH^+}}{cps^{norm}_{H_3O^+} + cps^{norm}_{H_2O.H_3O^+}} - \frac{cps^{norm}_{R_iH^+}(zeroair)}{cps^{norm}_{H_3O^+} + cps^{norm}_{H_2O.H_3O^+}(zeroair)} \right) \times S_i \quad (1)$$

159 $$cps_{\mathrm{R_iH^+}}^{norm} = \frac{\mathrm{TR_{H_3O^+}}}{\mathrm{TR_{R_iH^+}}} \times cps_{\mathrm{R_iH^+}}$$

160 where U_{drift} is the voltage of the drift tube (V), T_{drift} is the drift tube temperature in Kelvin (K),
161 $cps_{\mathrm{R_iH^+}}$ is the count rate (cps) of the product ion, $cps_{\mathrm{H_3O^+}}$ and $cps_{H_2O.H_3O^+}$ are the count rates of
162 the source ion and the first water cluster, k is the protonation rate constant assumed identical for
163 all compounds ($2.5\ 10^{-9}$ cm^3 molecule^{-1} s^{-1}), *norm* stands for normalized, $TR_{H_3O^+}$ is the
164 transmission factor for H_3O^+, $TR_{R_iH^+}$ is the mass-dependent transmission factor for the
165 protonated compound R_i, p_{drift} is the pressure in the drift tube, and S_i is the normalised sensitivity
166 of the analyzer. Here $zeroair$ stands for the count rates measured for zero air under the same
167 conditions of pressure, temperature and voltage. The standard transmission curve from the
168 supplier was used to compute the normalised counts per seconds $cps_{\mathrm{R_iH^+}}^{norm}$ (Table B1, Appendix
169 B). The $cps_{\mathrm{H_3O^+}}^{norm}$ was computed from ion *m/z* 21.022 ($H_3{}^{18}O^+$) by multiplying by the isotopic
170 factor 487.56, the first water cluster was taken as the ion peak *m/z* 37.028. The number
171 $1.657\ e^{-11}$ is a constant specific to the instrument, accounting for the reaction time in the drift
172 tube and detailed in Appendix B.

173 **2.4. Mixing ratio calibration and uncertainties**

174 S_i was determined as explained in Gonzaga et al. (2019), section 2.9: a standard cylinder
175 containing 102 ppbv of benzene, 104 ppbv of toluene, 130 ppbv of ethylbenzene and 336 ppbv of
176 xylene (122 ppbv Ortho, 121 ppbv Meta, 123 ppbv Para; BTEX, Messer) was diluted with
177 synthetic air. S_i was then computed as the slope between measured mixing ratios as computed by
178 equation 1 when S_i=1, and the mixing ratio prescribed by the dilution system. Assuming that the
179 protonation rate constant was similar for all compounds a single S_i was computed ($S_i = 2 \pm 0.15$)

for all compounds except methanol for which a comparison with another PTRMS itself calibrated for methanol was used to determine $S_{methanol} = 15$. However, acknowledging that assuming an identical protonation rate constant k, and hence a single S_i for all compounds may lead to systematic errors, we evaluated this potential bias in the computed concentrations. To do so, we computed the ratio $S_i / S_{toluene}$, using data from another experiment performed with the same instrument the year before (data from Loubet et al. 2021), as well as the using data from the literature (Koss et al. 2018), with an instrument similar to ours, though not exactly the same. This exercise (Table B2) shows that for most compounds the systematic error made by assuming a single *k* is limited to less than 40% error, which is the range expected from theoretical estimations of k. However, for ethanol, formaldehyde, methanol and propene, the bias may be high (from ~3 to ~40), with a tendency to underestimate the actual mixing ratio. For methanol, a specific calibration was performed in this study against another PTRMS which was itself precisely calibrated. For the ethanol, formaldehyde and propene the bias may have been be large, and especially for ethanol. For monoterpenes there might also be large differences in $S_{methanol}$, but this may be specific to the species composition at each site, since each monoterpene may fragment in different patterns (Tani et al., 2003).

Since no specific calibration was performed, except for toluene and methanol during this study, we did not correct our data using the $S_i / S_{toluene}$ shown in table B2, but rather proposed alternative estimates in standard emission factors in the discussion section. Nevertheless, the calibration data from Koss et al. (2018 and Loubet et al. (2021) also provided some estimates of the overall uncertainty on the mixing ratio determination, which is also provided in Table B2 as a relative standard deviation. Assuming these relative uncertainties would be similar in different

202 experiments, we estimated the uncertainties in mixing ratios would have been on average 15%
203 and ranged from 1% to 100%.

204 **2.5. Uncertainties in calculated concentrations due to humidity**

205 It is well documented that PTR-MS sensitivity is strongly influenced by relative humidity (RH),
206 resulting in uncertainty in the calculated BVOC concentration (Baasandorj et al., 2015; Christian
207 et al., 2004; Feilberg et al., 2010; Kari et al., 2018; Thomas Karl et al., 2003; Pang, 2015;
208 Steinbacher, 2004). Such humidity influence can lead to either an overestimation or an
209 underestimation of the BVOC concentrations depending on the compounds considered and the
210 setting of other parameters of the PTR-MS, notably the E/N (ratio of electric field to gas density).
211 For example, several studies show a significant underestimation of formaldehyde concentrations,
212 ranging from a factor of 3 to 5, by PTR-MS with increasing humidity (Christian et al., 2004;
213 Thomas Karl et al., 2003; Steinbacher, 2004; Vlasenko et al., 2010). Baasandorj et al. (2015)
214 showed that the sensitivity of PTR-MS to acetic acid decreases with humidity when the collision
215 energy in the PTR-MS drift tube is high (E/N >125 Td). In contrast, when E/N is low, a clear
216 increase in the sensitivity of PTR-MS to acetic acid with humidity was observed by the authors.
217 Changing the water vapor pressure from 0.61 to 3 kPa at E/N 142 Td, resulted in a significant
218 decrease of 30% in the sensitivity of the PTR-MS to acetic acid (Baasandorj et al., 2015) due to
219 an increase of the fragmentation of this compound at high RH (Feilberg et al. , 2010). Assuming
220 Baasandorj et al. (2015) results could be transposed to our setup, we evaluated that this effect
221 would lead to an underestimation of the deposition flux of acetic acid of 35% on average.
222 Regarding GLVs compounds, Pang et al. (2015) showed a linear increase in sensitivity with
223 increasing humidity. Sensitivities increased between 20% and 35% when the humidity increased
224 from 0 to 70%. In contrast, mono- and sesquiterpenes do not appear to show significant humidity

dependence. In general, a slight increase in sensitivity was reported for some terpenes ranging from 1% to 4% over a wide range of relative humidity from 0% to 100% (Tani et al. 2004).

In order to minimize the effect of humidity on PTR-MS sensitivity, the chambers remained open during non-sampling periods to avoid overheating and plant over-transpiration. However, even with these precautions, changes in humidity in the sampled air may have introduced uncertainties in the calculated concentrations as discussed in this section.

2.6. Leaf area and dry-weight estimations

Wheat plants were no longer growing during the measurement period. Thus, the leaf area was considered constant throughout the experiment, since senescence did not induce large changes according to visual inspection. Leaf area was determined by plant harvesting at the end of the experiment and subsequent scanning and image analysis using IMAGEJ®. Dry weight (g) was obtained after placing the plant organs (leaves and fruits) for 48 hours in a stove at 80°C.

Table 1 Wheat dry weight (DW) and leaf area in each chamber at the end of the experimental period.

	Ear DW (g)	Leaf DW(g)	Biomass DW(g)	Leaf Area (m^2)
Wheat 1	21.2	3.3	24.5	0.06
Wheat 2	16.4	2.0	18.4	0.05

2.7. BVOC fluxes

As detailed in Niinemets et al. (2011), after chamber closure, the time necessary to reach the chamber steady-state can be estimated as 4 times the half-time of complete air replacement of the chamber. According to Niinemets et al. (2011) this time allows for 94% of full system response and it is a satisfactory approximation of the time required to reach a steady-state:

(2)

244 $$t_{ss} = 4\frac{\ln(2)\,V}{Q_V}$$

245 where Q_V is the volumetric air flow rate ($m^3.h^{-1}$) into the chamber and V is the chamber volume
246 (m^3). Our system parameters gave a stabilization time t_{ss} of about 7 minutes. We hence chose to
247 start measurements 10 minutes after chamber closure to ensure sufficient time for mixing and to
248 facilitate overall automation. PTR-Qi-TOF-MS measurements in each sampling line (inlet and
249 outlet air) took 1 minute, of which only the last 30 seconds were kept to allow signal
250 stabilization. Each chamber was opened again immediately after the end of measurements.
251 Measurements were taken every hour and so during a complete cycle each chamber remained
252 closed for 12 minutes of 1 hour.

253 The flux of each BVOC was calculated based on the concentration difference of the compound
254 measured in the outlet and inlet air of the chambers:

255 $$\mathrm{F} = \frac{\left(C_{\mathrm{out}}(VOC) - C_{\mathrm{in}}(VOC)\right) Q_V}{DW} \quad (3)$$

256 where F is the BVOC flux expressed in $\mu g.g^{-1}(biomass\ dry\ weight).h^{-1}$, $\mathrm{C_{out}}(VOC)$ and
257 $\mathrm{C_{in}}(VOC)$ are the outlet and inlet BVOC concentrations in $\mu g\ m^{-3}$, DW is the dry biomass of
258 plants in g (leaves and/or ear organs) inside the chamber, and Q_V is expressed in $m^3.h^{-1}$.

259 **2.8. Net photosynthesis**

260 Equation 3 (Von Caemmerer and Farquhar, 1981) was used to calculate the net photosynthesis:

261 $$Pn = \frac{\left(\chi_{\mathrm{in}}(CO_2) - \chi_{\mathrm{out}}(CO_2)\right) Q_m}{S} \quad (4)$$

where Pn is the net photosynthesis (µmol CO_2 m^{-2} s^{-1}), $\chi_{in}(CO_2)$ and $\chi_{out}(CO_2)$ are the CO_2 dry molar ratios from chamber inlet and outlet air, respectively (µmol CO_2 mol^{-1}), S is the leaf area (m^2), and $Q_m = V_{mol}(air) \times Q_V$ is the molar air flow rate ($mol.s^{-1}$).

2.9. Standard emission factors

As discussed in section 1, BVOC emissions are strongly affected by environmental factors and in particular temperature and light, which are hence always used in models as drivers to simulate BVOC emissions. However, individual BVOC species can respond differently to temperature and light. Some compounds depend only on temperature, notably those originating from storage pools, while others depend on light and temperature, in particular when linked with the photosynthesis pathway, such as isoprene. In order to normalise measured emissions for temperature and light, the standard emission factor was calculated by fitting the following equation from Guenther et al. (1995):

$$F = E_S \, C_L \, C_T \tag{5}$$

Where E_S is the standard emission factor and F is the measured BVOC flux, both expressed in µg g_{DW}^{-1} h^{-1}. C_T and C_L are coefficients describing respectively the temperature and light dependency of the flux. For BVOC compounds depending on light and temperature (model TP), such as isoprene, C_T and C_L were computed as:

$$C_T = \frac{\exp\left[\frac{C_{T1}(T - T_S)}{R\,T_S T}\right]}{1 + \exp\left[\frac{C_{T2}(T - T_M)}{R\,T_S\,T}\right]}, \qquad C_L = \frac{\alpha\, C_{L1} \mathrm{PAR}}{\sqrt{1 + \alpha^2 \mathrm{PAR}^2}} \tag{6}$$

with the empirical constants $C_{T1} = 95000$ J mol^{-1}, $C_{T2} = 230000$ J mol^{-1}, $T_M = 314$ K, α = 0.0027, C_{L1}= 1.066, and where T is the leaf experimental temperature (K), T_S is the leaf

temperature at standard conditions (303 K), R the gas law constant (8.314 1 J mol^{-1} K^{-1}), and PAR the photosynthetically active radiation (PAR) flux (μmol_{photon} m^{-2} s^{-1}). For BVOC species depending only on temperature (like monoterpenes, model Tonly), $C_L = 1$ and C_T was computed as:

$$C_{\mathrm{T}} = \exp\left(\beta(T - T_S)\right) \quad (7)$$

with the empirical constant $\beta = 0.09K^{-1}$.

We fitted the measured flux for each individual BVOC with the two proposed dependency models (eq. 5 and 6) and selected the model with the highest R^2 coefficient to estimate the standard emission factors (SEF) at each developmental stage. We noticed that for the most exchanged BVOC species the temperature dependency model C_T showed most of the time the best R^2 (see Appendix C).

2.10. BVOC tentative identification

Identification was attempted with the software PTR-MS VIEWER 3 (Ionicon) coupled with the NIST database. Exact identification of all ions presented in this study was not possible. Indeed because of the principle of mass spectrometry, distinction of compounds having the same molecular weight (isobaric) or the same chemical formula (isomeric) was not possible. Thus, some compounds have been suggested for these masses based on the literature, and in comparison with GC-MS measurements in a campaign conducted in 2018 at the same farm (Kammer et al., 2019). The concentration of the *m/z* 43.018 compound strongly correlated (0.98 correction factor during ripening and senescence) with the *m/z* 61.029 (acetic acid), which strongly suggest that the *m/z* 43.018 is a fragment of acetic acid. Based on the linear regression slope between *m/z* 43.018 and *m/z* 61.029, a correction factor of 2.7 was worked out for acetic

304 acid concentrations. However, due to uncertainties in the evaluation of this correction factor, we
305 did not systematically apply this correction factor to the data, but rather proposed an alternative
306 evaluation of the acetic acid standard emission factor.

307 **Table 2. List of ions detected in this study for which a tentative identification is proposed. The measured**
308 **mass-to-charge ratio (*m/z*) of the ions, their potential compounds and/or chemical formula as well as the**
309 **measured *m/z* peak deviation from the theoretical *m/z* are presented. In bold compounds that are discussed in**
310 **this study due to their relevant contribution to the overall fluxes or commonly cited in literature.**

Suggested compound	*m/z*	Peak deviation	Tentative chemical formula
Formaldehyde	31.018	0.0000	$(CH_2O)H^+$
Methanol	**33.034**	**0.0000**	**$(CH_4O)H^+$**
Isoprene (frag.); Propyne	**41.038**	**0.0000**	**$(C_3H_5)^+$; $(C_3H_4)H^+$**
Acetonitrile	42.034	0.0000	$(C_2H_3N)H^+$
Ketene; Acetic acid (frag.) [a]	**43.018**	**0.0002**	**$(C_2H_2O)H^+$; $(C_2H_3O)^+$**
Propene	43.054	0.0010	$(C_3H_6)H^+$
Acetaldehyde	**45.033**	**0.0010**	**$(C_2H_4O)H^+$**
Formic acid	47.014	0.0008	$(CH_2O_2)H^+$
Ethanol	47.049	0.0011	$(C_2H_6O)H^+$
Methanethiol	49.011	0.0000	$(CH_4S)H^+$
Acrolein	57.034	0.0005	$(C_3H_4O)H^+$
Hexenal (frag.); Butanol (frag.)	**57.069**	**0.0009**	**$(C_4H_8)H^+$**
Acetone	**59.048**	**0.0011**	**$(C_3H_6O)H^+$**
Acetic acid [a]	**61.029**	**0.0004**	**$(C_2H_4O_2)H^+$**
Triazole [b]	69.032	0.0004	$(C_2H_2N_3)H^+$
Isoprene ; Methyl butenol (frag.)	**69.069**	**0.0001**	**$(C_5H_8)H^+$**
Methyl vinyl ketone ; methacrolein	71.049	0.0011	$(C_4H_6O)H^+$
Pentene	71.084	0.0015	$(C_5H_{10})H^+$
Propenoic acid	73.028	0.0014	$(C_3H_4O_2)H^+$
Methyl ethyl ketone (MEK)	**73.064**	**0.0018**	**$(C_4H_8O)H^+$**
Benzene	79.051	0.0012	$(C_6H_6)H^+$
Hexene ; Monoterpenes (frag.); Hexenal (frag.)	81.070	0.0009	$(C_6H_8)H^+$
Methylfuran	83.048	0.0001	$(C_5H_6O)H^+$
Hexenol (frag.); Hexadiene	**83.084**	**0.0015**	**$(C_6H_{10})H^+$**
Pentenone	85.062	0.0018	$(C_5H_8O)H^+$
Pentenol; Pentanal; Pentanone; Methyl butenol	87.078	0.0034	$(C_5H_{10}O)H^+$
Iron dihydroxide	90.946	0.0017	$(FeH_2O_2)H^+$
-	91.053	0.0012	$(C_7H_6)H^+$; $(C_7H_7)H^+$
Hexenal; Hexenone	**99.079**	**0.0034**	**$(C_6H_{10}O)H^+$**
Heptene	99.114	0.0008	$(C_7H_{14})H^+$
Pentenoic acid; ISOPOOH	101.058	0.0007	$(C_5H_8O_2)H^+$
Hexenol	**101.092**	**0.0041**	**$(C_6H_{12}O)H^+$**
Methacrylicperoxy acid	103.039	0.0010	$(C_4H_6O_3)H^+$
Pentanoic acid	103.074	0.0024	$(C_5H_{10}O_2)H^+$
Styrene	105.068	0.0010	$(C_8H_8)H^+$
Benzaldehyde	107.047	0.0001	$(C_7H_6O)H^+$
-	**108.957**	**0.0003**	**NO_4P^+** [b]**; CO_4S**
Octadiene	111.114	0.0028	$(C_8H_{14})H^+$
Santene	123.114	0.0018	$(C_9H_{14})H^+$
- [c]	**125.959**	**0.0003**	**$(NO_5P)H^+$**
Methylbenzoate	137.059	0.0017	$(C_8H_8O_2)H^+$

8-Azaadenine		0.0010	$(C_4H_4N_6)H^+$
Monoterpenes	**137.132**	**0.0015**	**$(C_{10}H_{16})H^+$**
Isofraxidin; 3-(Acetyloxy) benzoic acetic	223.055	0.0009	$(C_{11}H_{10}O_5)H^+$
-	225.035	0.0006	$(C_{10}H_{18}O_6)H^+$

a. The m/z 43.018 fragment of acetic acid led to a correction factor of 2.7 of acetic acid concentrations and fluxes. This correction was not systematically applied but rather used to evaluate an alternative standard emission factor for acetic acid in the discussion section.
b. Triazoles are documented degradation products of "azole" fungicides which were used on the wheat during the spring and are known to be persistent in the ecosystem for several months.
c. Isotopic pattern consistent at m/z +1 and m/z +2

2.11. Wheat plant developmental periods

The experiment started at the maturation of the seeds. The beginning of plant senescence was identified by a gradual decrease in the rate of photosynthesis as discussed in Taiz et al. (2015) or Mozaffar et al. (2018). Three developmental periods have been distinguished: (1) Ripening, during which the plants have constant photosynthetic activity, (2) Senescence 1, when the photosynthesis decreases gradually but plants remain green and (3) Senescence 2, characterized by no photosynthetic activity and plants turning progressively yellow (chlorosis) (Figure 1). Chlorosis occurred from Jun 21st to 29th. Afterwards, the plants were cut at the base (about 20 cm above the ground) simulating a harvest and measurements continued for 4 days.

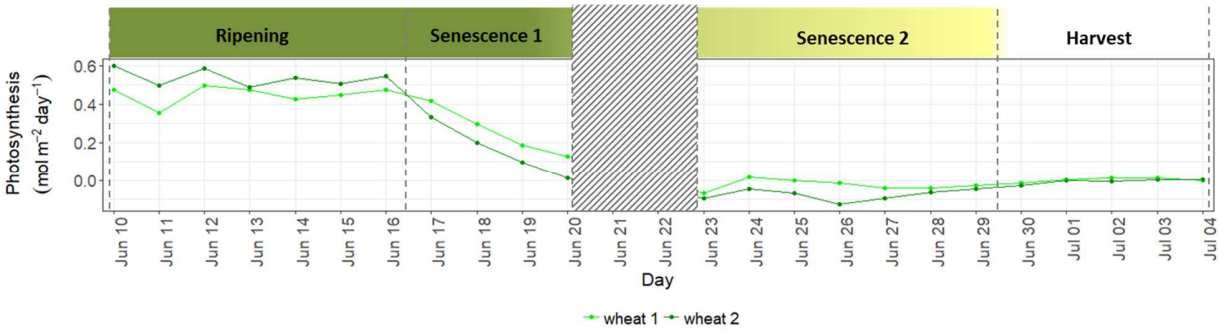

Figure 1. Temporal evolution of daily photosynthesis rate (mol CO2 m^{-2} day^{-1}) for the two wheat plants over developmental stages. The striped zone corresponds to missing data.

2.12. Statistical analyses

Data analyses were performed with R (RStudio 1.1.463, R version 3.5.2). A Student's t-test was performed in order to evaluate whether the mean BVOC fluxes were significantly different from zero. The fluxes were first averaged per day for each ion before performing the t-test to limit temporal correlation. Similarly the mean fluxes and 95% confidence intervals for each ion were computed as follows. For each day, ion and plant, the daily mean emission was first computed. Then the averaged daily emission and the corresponding confidence interval were computed over all days and both plants.

2.13. Comparison with eddy covariance fluxes obtained in a nearby field the year before

Given the limited number of replicates of our experimental design with only two wheat plants, no statistically significant differences could be assessed to determine if there is a real effect of plant development stages on BVOC emissions. To overcome this difficulty, we used Eddy covariance (EC) fluxes measured with the same instrument at the same site one year prior to the present study. These measurements by EC were taken during the same developmental stages and on the same soil. These data were compared with the emission factors reported here and their variations with plant developmental stages. These data were reported by Loubet et al. (2021), and are referred to as the COV3ER-2016 dataset in the following sections. The data were taken from the repository associated with this publication (https://doi.org/10.15454/IRZ9XX), and are not detailed here.

Similarly to what was done in this study with net plant photosynthesis (Figure 1), ripening, senescence 1, and senescence 2 periods were determined based on measured net ecosystem exchange (Appendix D). For each of these periods, the standard emission factors estimated in this

study were used to compute the SEF-based whole plant VOC emissions using air temperature and incoming photosynthetically active radiation as measured in COV3ER-2016 and equations 5-7. These SEF-based whole plant VOC emissions were compared to hourly measured fluxes in COV3ER-2016 which were scaled to µg g^{-1}(DM) h^{-1} by multiplying the fluxes in nmol m^{-2} s^{-1} by $ion\_mass \times 3600/1000 \times AGB$, where AGB is the total above ground biomass that was 1224 g m^{-2} during that period.

2.14. OH reactivity

In order to evaluate the impact of the measured BVOC emissions, and their change with plant stages, on the atmospheric chemistry, we evaluated their potential OH reactivity. Once emitted, BVOCs can reduce the atmospheric reactivity mainly through their reaction with the OH radical, which leads to an accumulation of other compounds such as methane. As the reactivity with the OH radical strongly depends on the compound, the impact on atmospheric reactivity depends not only on the emissions in terms of quantity but also on its composition. Thus, in order to evaluate this impact, measured BVOC concentrations of the compounds identified in Table 2 were used to calculate a theoretical OH reactivity (*cROH* for calculated OH reactivity), which consists of the sum of the reaction frequencies of all chemical compounds with OH. In practice *cROH* was calculated as the sum of the products of each compound concentration $[X_i]$ (in molecule cm^{-3}) by the reaction rate coefficient of this compound with OH, k_{OH+X_i} (in cm^3 $molecule^{-1}$ s^{-1}):

$$cROH = \sum k_{OH+X_i}[X_i] \quad (8)$$

This calculated OH reactivity represents the expected total loss rate of OH, which is the inverse of OH lifetime (s^{-1}). The relative uncertainty in *cROH* was computed as the sum of relative

uncertainties in concentration (assumed equal to that on mixing ratio) and in k_{OH+X_i} which was retrieved from the literature (see Table G1, Appendix G for details on k_{OH+X_i}).

3. Results

3.1. Meteorological variation during the campaign

Air temperature, photosynthetically active radiation (PAR) and air relative humidity (RH), presented similar temporal variability for both wheat chambers, with a clear diurnal dynamics pattern (Figure 2). On average, the air temperature during measurements was 2.3 °C larger inside the chambers than above the canopy during daytime, but maximum differences reached 10°C, denoting a noticeable impact of chambers on the plant microclimate. Maximum diurnal temperatures remained in general between 30 and 40°C during the entire measurement period, exceptions are: June 19th and 20th, during which the temperature increased above 40°C; and July 01st, during which the temperature remained below 30°C, concomitantly with a low PAR. It can also be noted that the period from June 27th to July 2nd was marked by poor weather conditions with some rainfall events. During that period, temperature presented a less pronounced diurnal pattern with smaller temperature ranges. The PAR transmissivity of the chamber was evaluated to be 89% (Pape et al., 2009). During daytime, PAR was on average 264 µmol m^{-2} s^{-1} higher above the canopy than inside the chambers. This was expected due to the presence of plants surrounding the sensor in the chamber and the chamber itself. The relative humidity inside the chambers was close to the one measured above the canopy (0.1 to 1.8% higher inside the chambers during daytime) and hence was representative of the ambient air. Although the chambers were affected by temperature, it is important to keep in mind that they remained open most of the time and

394 therefore the conditions inside the chambers were affected only during the short periods of
395 closure (12 minutes every hour).

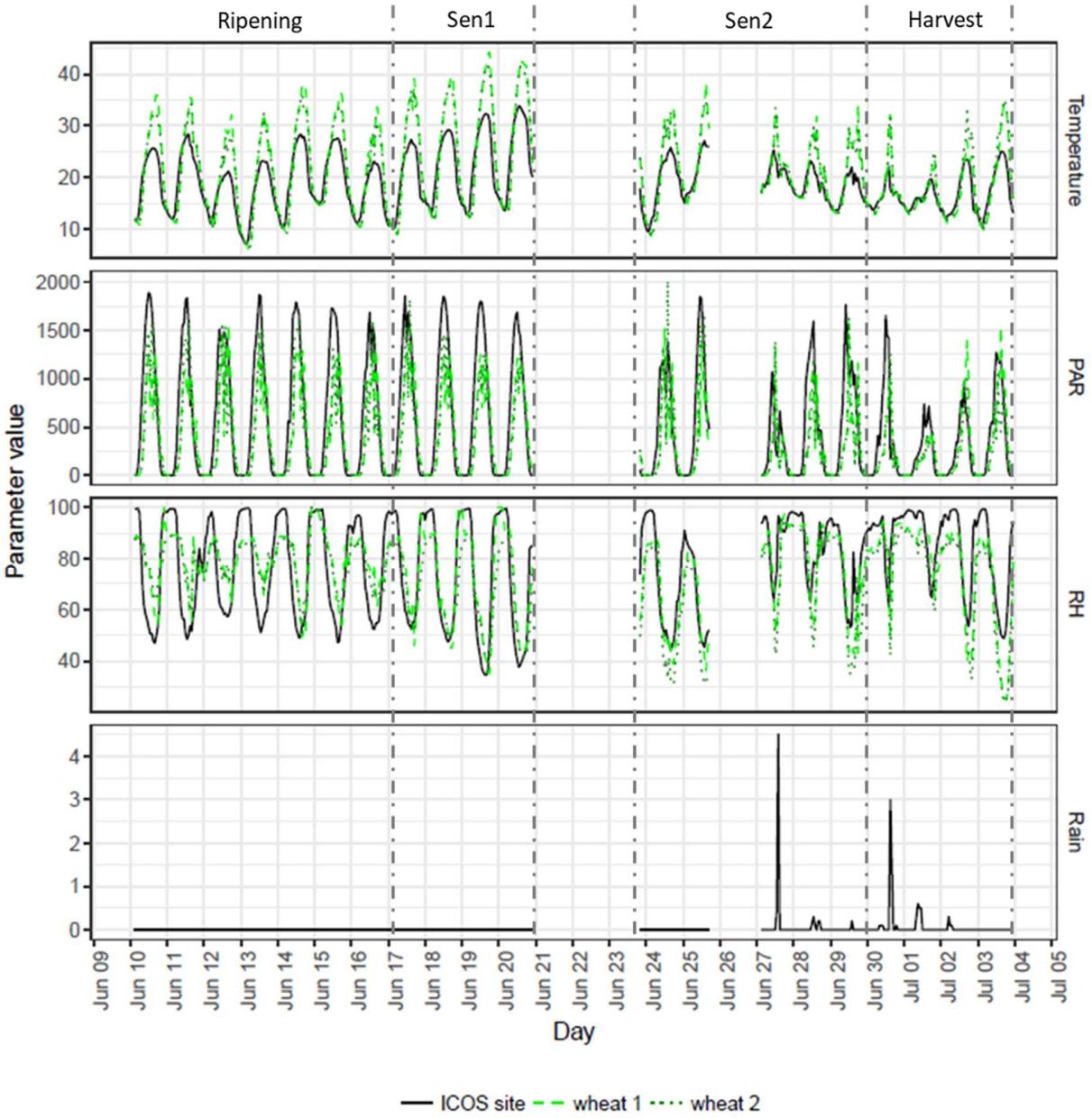

396

397 **Figure 2 Environmental conditions measured inside each chamber (*Wheat_1*, and *Wheat_2*) and at 1 meter**
398 **above canopy (ICOS site). PAR is given in µmol m^{-2} s^{-1}, relative humidity (RH) in %, rain in mm and**
399 **temperature in °C.**

400

3.2. BVOC fluxes variation between developmental wheat periods

The overall fluxes for the different developemental periods were generally well reproduced (qualitatively and quantatively) between the two wheat plants (Figure 3). Althought the overall BVOC emission rate was generally higher for *Wheat_2* plant, compared to *Wheat_1*, especially during *Ripening* (emission rate about twice as large), it remained of the same order of magnitude. For both plants the overall emission rate increased considerably during the first period of senescence (*Sen1*), decreased slightly during the seconde period of senecence (*Sen2*) and then declined abruptly after harvest. Net deposition was also observed, ocurring mainly during *Ripening* and *Sen1*, and after harvest in the case of methanol.

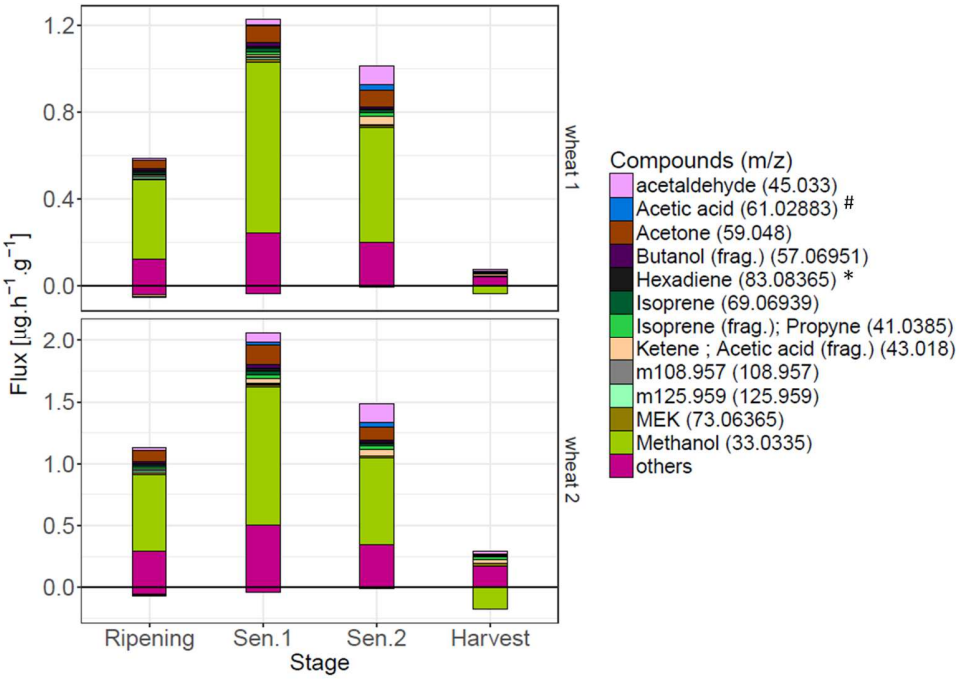

Figure 3: Overall BVOC fluxes and composition for each developmental period of wheat plants. We show for comparison all 12 compounds that were among the 5 most exchanged during at least one developmental stage. 7The category "others" includes the fluxes of all the other detected ions. # Acetic acid not corrected for m/z 43 fragment. * Hexadiene could also correspond to a fragment of hexenol, a green leaf volatile (GLV).

3.2.1. Qualitative BVOC fluxes variation

The most exchanged compounds for each developmental period and their contribution to overall fluxes is depicted in Figure 3. All compounds that were among the top 5 compounds for each developmental stage were selected, which represented 12 compounds in total. Together, these major compounds represented about 80% of the net overall fluxes for each period, except harvest. It can be noted that the composition of these most emitted compounds varies according to the stage of development. In general, the most emitted compounds were: methanol, acetaldehyde, acetic acid and acetone. Methanol was the most emitted compound for all periods, excepted harvest, contributing to 60%, 59% and 49% of the overall BVOC flux during *Ripening*, *Sen1* and *Sen2* (average of both chambers), respectively (see Appendix E). During *Ripening*, acetone was the second most emitted compound, contributing 9% to the overall fluxes. During senescence, acetone, acetaldehyde and acetic acid were the most emitted compounds after methanol, contributing, respectively 8%, 3% and 1% to the overall net fluxes during *Sen1* and 8%, 10%, 3% during *Sen2* (see Appendix E). The remaining most emitted compounds each presented a minor contribution to the overall fluxes. These ions were: *m/z* 69.069 (Isoprene; Methyl butenol fragment), *m/z* 73.064 (Methyl ethyl ketone), *m/z* 83.084 (Hexadiene), *m/z* 108.957 (NO_4P) and *m/z* 125.959 (NO_5P). The likely fragments of acetic acid, isoprene and butanol fragments, at *m/z* 43.018, 41.039, 57.069, respectively, also appeared among the most exchanged compounds. If m/z 43.018 is accounted as acetic acid, this increases its contribution to the overall flux, especially during *Sen2* where it reaches 7.3% of the overall fluxes (Appendix E). After harvest, no compounds made a significant individual contribution to overall emissions, apart from methanol which was mainly taken up and represented around 36% of the overall flux.

3.3. Fluxes temporal variation for individual BVOC

In general, the temporal fluxes variation of the most emitted BVOCs showed similar trends for both wheat plants, despite a few differences being observed mostly after harvest (Figure 4). However, *Wheat_2* showed emission rates higher than *Wheat_1* for all compounds, except during *Sen2* for a few compounds. This difference was small for methanol but sometimes reached a factor of 2 for hexadiene, acetone, acetaldehyde and isoprene. Clear diurnal dynamics were observed for most compounds throughout the whole measurement period, except for acetic acid during *Ripening* and *m/z* 108.957 and 125.959 ions during *Sen2*.

Several temporal trends can be observed among the different compounds. For example, some compounds, such as methanol, acetaldehyde, acetone, isoprene, hexadiene and hexanal, presented a gradual increase in emission rates during *Sen1*, while for *m/z* 108.957 and 125.959 ions, emission rates gradually decreased at the beginning of senescence and reached a minimum during *Sen2* and after harvest. Some small amounts of deposition were also noticed for some compounds including acetaldehyde and acetic acid, occurring mainly during *Ripening* and *Sen1*. An important deposition of methanol was observed mainly after harvest (Figure 4).

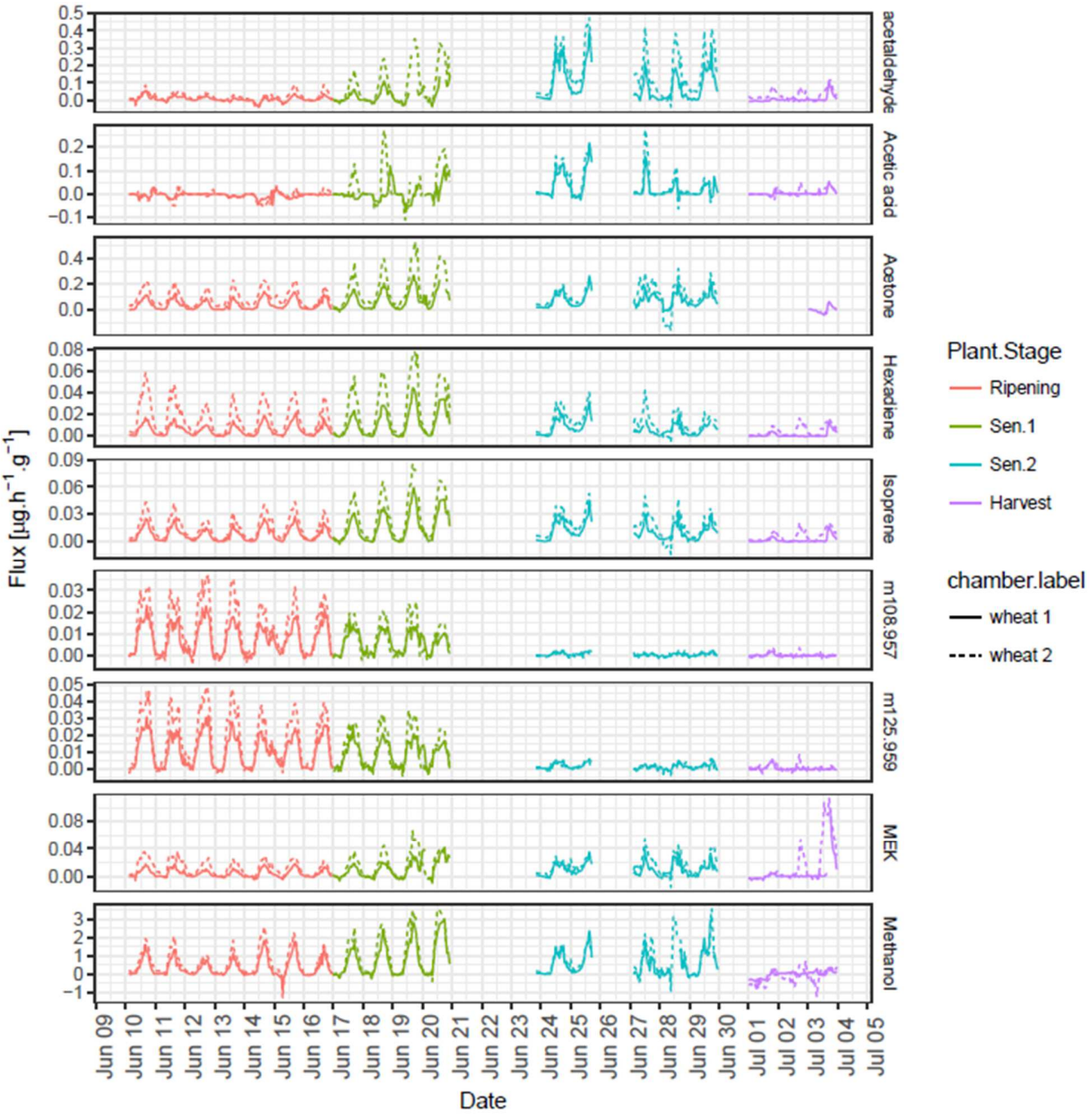

Figure 4: Fluxes variation during the measurements period for some of the most exchanged compounds. Acetic acid was not corrected for m/z 43 fragment in this figure. Hexadiene could also correspond to a fragment of hexenol, a green leaf volatile (GLV).

In order to better analyze the BVOC flux variation during the investigated periods, flux statistics over each stage and for each major compound are depicted in Figure 5. Overall, most compounds presented a larger averaged emission during *Sen1*. However we observed 5 types of behaviors: (i) a significant increase in average emission rates from *Ripening* to *Sen1*, followed by a significant

460 decrease during *Sen2*, and an abrupt decrease during harvest. This behavior was observed for
461 methanol, isoprene, hexenal, hexenone, hexadiene and *m/z* 101.092. In the case of methanol, the
462 flux turned from a net emission to a net deposition during harvest; (ii) a significant increase from
463 *Ripening* to *Sen1*, but a further increase during *Sen2*, and a drastic decrease during harvest. Such
464 was the case for acetaldehyde and acetic acid; (iii) a significant increase from *Ripening* to *Sen1*,
465 no significant variation during *Sen2*, and a decrease during harvest. This behavior concerns
466 acetone and MEK, the latter of which showed a peak in emissions two days after harvest; (iv) *m/z*
467 108.957 and 125.959 showed a significant decrease from *Ripening* to *Sen1*, from *Sen1* to *Sen2*,
468 and from *Sen2* to harvest; (v) no significant variation from *Ripening* to *Sen1* and to *Sen2*, and a
469 significant decrease from *Sen2* to harvest, being the case for monoterpenes.

470 BVOC emissions from plants are known to depend strongly on temperature and light conditions.
471 Given the large variation of these climatic factors between the different periods investigated, the
472 flux differences observed between the different periods could be either due to plant development
473 or to variation in temperature and light conditions. The standard emission factors (SEF),
474 calculated for each compound during each developmental stage (Figure 5) can be seen as fluxes
475 at standard conditions of temperature and light. Thus, the SEF allow comparing the fluxes
476 between the different developmental stages while eliminating the effects of temperature and light.
477 Figure 5 shows that SEF varied with plant development, but SEF variations were often different
478 when compared to the measured fluxes. Overall, SEF were higher during *Sen2*, contrary to the
479 measured fluxes which were either smaller or of similar magnitude to that during *Sen1*. Based on
480 SEF, different behaviors are identified: compounds for which SEF increased between periods
481 (acetaldehyde, acetic acid, acetone, isoprene, hexanal), those for which SEF decreased (*m/z*
482 108.957, 125.959 and monoterpenes), those for which SEF decreased during *Sen1* and then

increased during *Sen2* (methanol), and those for which only during *Sen2* SEF decreased (*m/z* 101.092) or increased (MEK), while for hexadiene SEF remained stable among all periods.

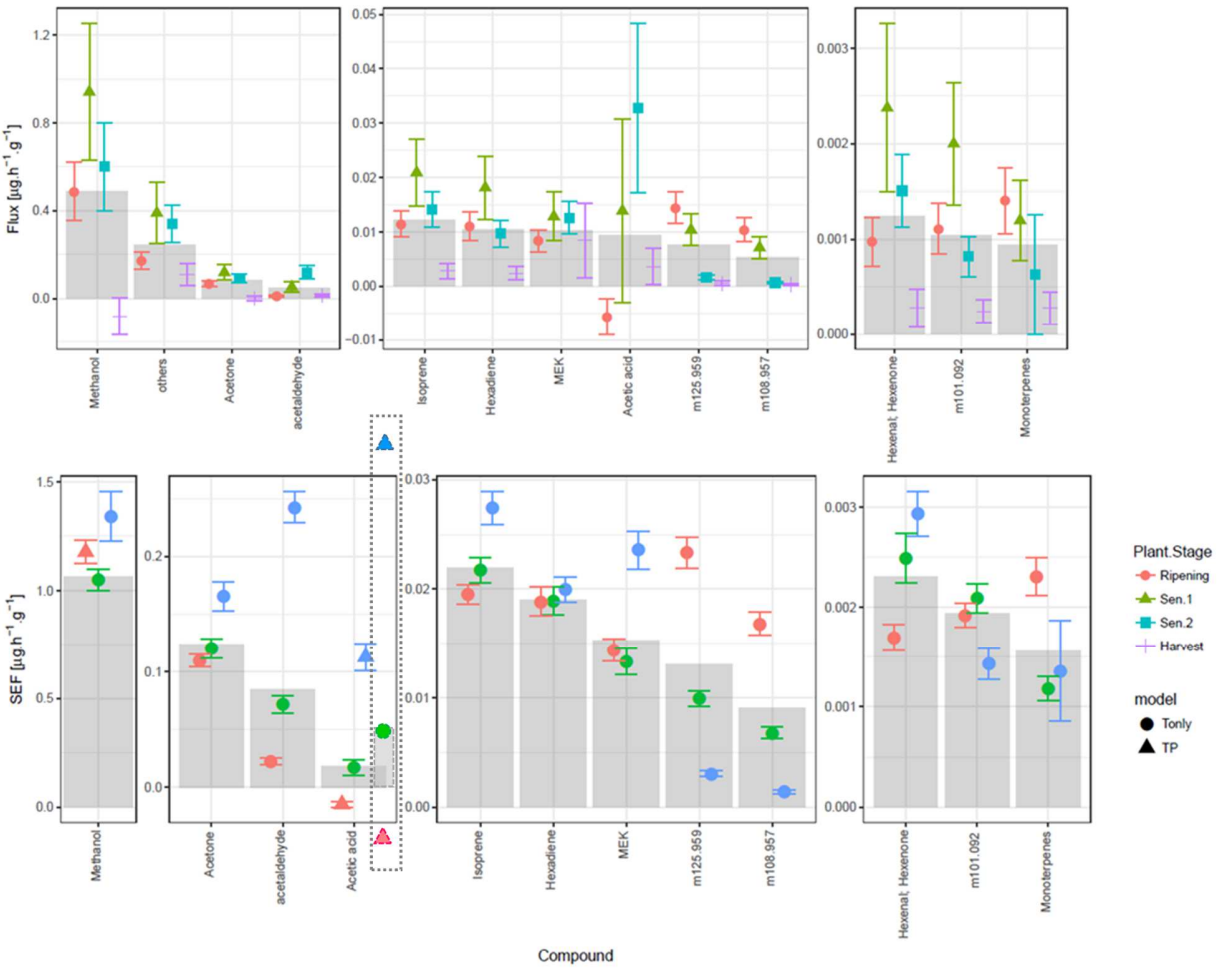

Figure 5. Top: Mean fluxes (µg g^{-1} h^{-1}) estimated for each developmental period (dots), corresponding 95% confidence interval (error bars), and mean fluxes over the entire measurement period (grey bar). Bottom: standard emission factor SEF at standard temperature (30°C) and light (1000 µmol m^2 s^{-1}) estimated for each developmental period (dots), corresponding 95% confidence interval (error bars), and SEF estimated for the whole measurement period (grey bar). SEF were obtained by fitting the measured flux with the temperature and light dependency (TP) or the temperature dependency only (Tonly) model given by (Guenther et al., 1995) as explained in the text. The model with highest R^2 was selected. The R^2 coefficients are provided in Appendix C. SEF are not shown for harvest since there was no plant left in the chamber, apart from a small portion of the plant stems. Compounds were grouped by similar scale of mean emission to facilitate visualization, only the y-scale changes between groups. Hexadiene could also correspond to a fragment of hexenol, a green leaf volatile (GLV). For acetic acid, an alternative evaluation of the SEF is given in the dashed rectangle, for which m/z 43 was considered a fragment of acetic acid.

3.4. Comparison of modelled VOC fluxes with eddy covariance fluxes in COV3ER-2016

The SEF-based whole plant VOC emissions compared overall quite well with the COV3ER-2016 whole ecosystem fluxes (Figure 6). This is especially true for acetone, during ripening and early senescence (*Sen1*), where with a slope of 0.8 and 1.1 in x-y regressions. Acetaldehyde SEF-based whole plant VOC emissions were lower than whole ecosystem fluxes during *Rip* and *Sen1* (by a factor of 5 to 2), while methanol plant fluxes were larger than whole ecosystem fluxes during the same period (by a factor of ~2). During maturation and chlorosis (*Sen2*) the SEF-based whole plant VOC emissions were systematically larger than COV3ER2016 whole ecosystem fluxes, by a factor of ~2. For acetic acid, the SEF-based whole plant VOC emissions were systematically larger than the whole ecosystem fluxes measured in 2016, although the orders of magnitude were similar during *Rip* and *Sen1*. See Appendix F for details on linear regressions.

Figure 6. Comparison between measured whole ecosystem VOC fluxes in COV3ER-2016 (red) and SEF-based whole plant VOC emissions as derived in this study (blue) over the ripening (Rip), and senescence periods (Sen.1 and Sen.2). Here acetic acid fluxes are not corrected for m/z 43 fragments in both datasets.

3.5. OH reactivity

ROH showed a diurnal variability (Fig. 6), with maxima during day-time and minima during night-time, following temperature and PAR profiles, and thus the variability of total BVOCs fluxes. Similarly to what was described in section 3.2.1 on BVOCs fluxes variation, ROH remained of the same order of magnitude for both wheat chambers, with higher values during *Sen1* (19th- 20th of June 2017). Average day-time ROH was similar for both plants with 2.4 ± 3.0-2.5 ± 2.4 s^{-1} for wheat 1 and wheat 2, respectively. Maxima of 13.6 and 12.7 s^{-1} were recorded for wheat 1 and wheat 2, respectively, at *Sen1*. Interestingly, higher values of ROH were recorded for wheat 1 compared to wheat 2 during *Sen2*. These values remain in the lower ranges of OH reactivity compared to other ecosystems, especially for measurements from dynamic chambers (Bsaibes et al., 2020; Kim et al., 2011; Nölscher et al., 2013; Sinha et al., 2008), bearing in mind that flow rates and chamber setups may modify the absolute values of the reactivity. We evaluated that the uncertainty in calibration factors may lead to potentially underestimating the OH reactivity by 50% with an overall uncertainty of 25% (Fig. 7).

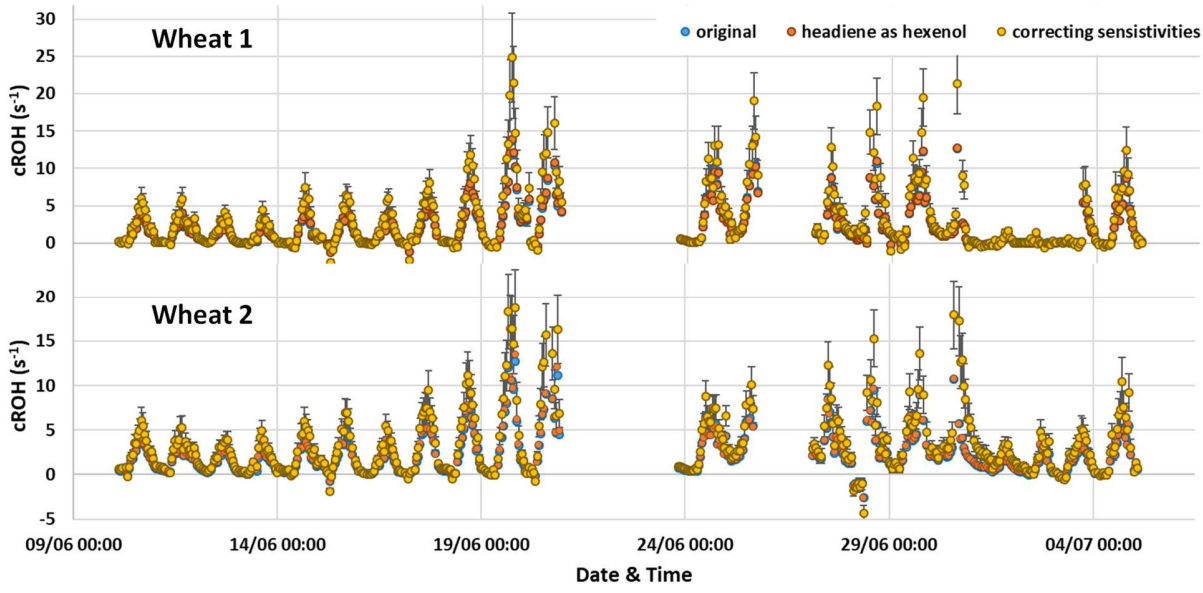

Figure 7. Calculated OH reactivity of the outlet air of the two wheat chambers. The effect of sensitivity corrections and considering hexadiene as an hexenol fragment were evaluated here.

Regarding the contribution of the main emitted compounds, methanol which was the most emitted compound in general, accounted for 12 - 17% of the cROH, acetaldehyde represented 16%, while other mainly emitted OVOCs accounted for much less (acetone 0.3- 0.4%, acetic acid 0.3- 0.4%, etc.). However, even though isoprene had a minor contribution to the overall flux, its contribution to cROH exceeded that of the mentioned OVOCs and reached 34- 36%, on average. Overall, senescence induced a marked increase in OH reactivity of up to 4-fold during senescence 1 and 2-fold during senescence 2 compared to the ripening period.

4. Discussion

4.1. Flux dynamics in relation with vegetation development

Grass species, which include wheat as the most widespread cultivated grass species, are known to emit relatively large amounts of oxygenated VOCs and some monoterpenes (Fukui and Doskey, 2000; Karl, 2009; Kirstine et al., 1998). Indeed, in this study oxygenated compounds dominated the BVOC exchanges for wheat plants, with methanol being the most emitted compound during all developmental periods followed by acetone, acetaldehyde and acetic acid (Figure 3). These findings are also in good agreement with recent literature studies on grass species including wheat (Bachy, 2018; Bachy et al., 2016; Gonzaga Gomez et al., 2019; Graus et al., 2013; Mozaffar et al., 2018).

Our study showed that many BVOC species were released in larger amounts as the plants entered senescence (*Sen1*), with emission rates decreasing thereafter as plant leaves turned yellow (*Sen2*). It has been suggested that, for some BVOC, higher emissions occurring during senescence may originate from the breakdown of cellular structures, cell organelles and macromolecules to

553 nutrients remobilization (Mozaffar et al., 2018; Rottenberger et al., 2005). In addition, chlorosis
554 is likely to increase BVOC diffusion through a degraded epidermal layer and cuticle (Mozaffar et
555 al., 2018). Thus, BVOC emissions are expected to rise as the leaves turn yellow and degradation
556 increases. However, our results showed a decrease in BVOC emissions during wheat chlorosis
557 (*Sen2*), which was probably due to unusual weather conditions during this period (i.e. heavy
558 rainfall and low temperatures). Indeed, emissions are likely to decrease when the temperature
559 decreases given the chemical properties of certain compounds, such as high solubility, or their
560 origin within plants, such as storage organs and enzymatic reactions (Cojocariu et al., 2004;
561 Hayward et al., 2004). Standard emission factors are in this case useful to distinguish the share of
562 flux variation due to temperature or endogenous plant variation. Most compounds showed an
563 increase in SEF during chlorosis (*Sen2*), except for *m/z* 101.092, 108.957, 125.959 and
564 monoterpenes. Thus, senescence induced higher emissions in wheat plants despite the presence of
565 rain, which may have increased deposition of soluble compounds (Bachy, 2018; Holzinger et al.,
566 2001).

567 In the following sections the most exchanged compounds are discussed more in details and
568 compared with literature findings.

569 **4.2. Compounds with increasing emissions during senescence**

570 **4.2.1. Methanol**

571 Methanol emission rates have already been found to increase with senescence for maize
572 (Mozaffar et al., 2018) and wheat plants (Bachy, 2018) in previous studies. In those studies,
573 emission rates of methanol increased slowly at the beginning of senescence reaching a maximum
574 emission rate during chlorosis. This is well in line with our results where methanol emissions

575 increased during the first phase of senescence (*Sen1*). However, emissions decreased during
576 chlorosis (*Sen2*), contrary to previous studies. Methanol emitted by plants is known to originate
577 from enzymatic reactions of pectin demethylation in the cell wall by Pectin Methyl Esterase
578 (PME) activity (Fall, 2003), a process occurring during growth but also during other events
579 impacting the cell wall structure such as senescence (Bachy et al., 2016; Karl et al., 2005;
580 Mozaffar et al., 2018). Thus, an increase in methanol emissions is expected with the progress of
581 senescence. Poor weather conditions during chlorosis, with a decrease in temperature and some
582 rain (Figure 2), hence explains the decrease in the measured methanol fluxes during chlorosis.
583 Indeed, due to the low temperatures, enzymatic activity was very probably inhibited, while
584 methanol solubility was improved during that period. Moreover, methanol being highly soluble
585 (≥100 mg/mL at 70° F; NTP, 1992) it is readily deposited on wet surfaces (Bachy, 2018;
586 Holzinger et al., 2001; Laffineur et al., 2012; Wohlfahrt et al., 2015). When normalized for
587 temperature, methanol emissions actually increased during chlorosis (*Sen2*), despite a probable
588 higher deposition due to the presence of wet surfaces.

589 **4.2.2. Acetone**

590 Increase in acetone emissions during plant senescence and biomass decay have previously been
591 reported in literature (Bachy, 2018; T. Karl et al., 2003; Mozaffar et al., 2018; Warneke et al.,
592 1999). Although acetone fluxes were bidirectional in the present study, average net flux always
593 resulted in net emissions for all the investigated periods. Contrary to our observations, in the
594 study of Bachy et al. (2018), acetone was on average deposited before the senescence of wheat
595 but was emitted during senescence. This difference may result from an acetone uptake by soil in
596 Bachy et al. (2016) since their measurements were at the ecosystem scale.

Schade and Goldstein (2001) found temperature to be the main environmental driver regulating acetone emissions. This is consistent with the decrease in acetone emissions during the chlorosis period, when temperatures were lower. Therefore, once normalized for temperature, emissions increased during chlorosis and exceeded those of the first senescence period.

Acetone is known to be produced in plants via the cyanogenic pathway (Fall, 2003). In this pathway, amino acids are converted into cyanogenic glycoside which is stored in the cell vacuoles. Impacts against cell wall structure, resulting from the senescence process, may enhance the contact of cyanogenic glycoside with β-glucosidase, a cell wall enzyme. This reaction leads to acetone cyanohydrin that subsequently reacts with another cell wall enzyme, hydroxynitrile lyase, to form acetone and hydrogen cyanide. This mechanism together with abiotic processes, through the Maillard reaction that was also reported for acetone (Warneke et al., 1999), may explain the observed increase in acetone emissions as senescence progresses. Indeed, Warneke et al. (1999) showed that the thermochemical Maillard reaction can produce oxygenated VOCs (OVOCs) even at typical ambient temperature (20-40°C). The wetting of leaves acts then as a desorption process that replaces OVOCs molecules attached to the surface of plants by highly polar water molecules in the aqueous phase. OVOCs can then be released to the air by Henry equilibrium. The wetting-drying cycle was shown to be an efficient emission process that can last several tens of cycles (Warneke et al., 1999). Since plants were not exposed to this wetting-drying cycle in our study, relative humidity may have contributed to desorption of OVOC attached to the plants surface as well demonstrated by Mozaffar et al. (2018), either through a water microlayer on the plant surface or through interactions with polar water vapour molecules.

4.2.3. Acetaldehyde

The sharp increase in acetaldehyde emissions during leaf senescence in this study is in good agreement with previous studies on maize (Mozaffar et al., 2018), wheat (Bachy, 2018) and tree species (Rottenberger et al., 2005). Although acetaldehyde emissions from plants are highly dependent on temperature, (Bachy, 2018; Cojocariu et al., 2004; Das et al., 2003; Hayward et al., 2004; Karl et al., 2005), acetaldehyde emissions increased during senescence, and mainly chlorosis, resulting from a senescence effect (Figure 5). Similarly to our observations, in the study of Bachy (2018) over a wheat field, acetaldehyde emissions increased from the early stages of senescence to reach higher levels during leaf chlorosis. In their study, acetaldehyde contribution to the overall BVOC emissions during beginning of senescence (2%) and chlorosis (6%) was similar to our findings, being 3% and 10% during *Sen1* and *Sen2*, respectively (see Appendix E). Mozaffar et al. (2018), investigating BVOC emissions from senescent maize leaves under controlled environmental conditions, found a delayed increase in acetaldehyde emissions, with a pronounced emission increase only 2 days after leaf chlorosis started. Although missing data do not allow a strict comparison of our study with Mozaffar et al. (2018), acetaldehyde emissions increased on 24th and 25th June (Figure 4), which is about 2 days after photosynthesis went down to zero and chlorosis started (Figure 1).

In terms of processes, the peroxidation of fatty acid by reactive oxygen species (ROS) might be the main mechanism for the production of acetaldehyde (Jardine et al., 2009) during the senescence period, as discussed by Mozaffar et al. (2018). It has also been suggested that acetaldehyde emissions could originate from internal pools (Hayward et al., 2004), and increased emissions during leaf senescence could result from the breakdown of cellular structures and

640 degradation of cell organelles (Rottenberger et al., 2005), although both studies were based on
641 tree species.

642 **4.2.4. Acetic acid**

643 The increase of acetic acid emissions during wheat senescence (Figure 5) observed here is
644 consistent with the study of Mozaffar et al. (2018) for maize leaf emissions. On the contrary, in
645 the study of Bachy et al. (2018), acetic acid fluxes resulted in an average net uptake during wheat
646 senescence. Given the ecosystem scale of their flux measurements, the authors invoked the
647 possible role of soil as an important acetic acid sink to explain the net uptake during senescence.
648 Indeed, it has been demonstrated that soil may act as an important sink for acetic acid (Bachy et
649 al., 2016). This hypothesis could explain the divergence between the ecosystem scale (Bachy,
650 2018) and plant scale studies (this study and Mozaffar et al., 2018). A further explanation would
651 be the ambient level of acetic acid. Indeed the deposition flux of a deposited compound will
652 increase with increasing its ambient level as is well known for instance with ammonia (Sutton et
653 al., 1995).

654 In terms of processes, the abiotic Maillard reaction was shown to be very effective for producing
655 acetic acid (Warneke et al., 1999). Mozaffar et al. (2018) showed good consistency of the
656 increase in acetic acid emissions with that mechanism during leaf senescence. Another process
657 that may favor acetic acid emissions is the decrease of leaf pH. Indeed, it has been demonstrated
658 that decrease in apoplastic pH leads to acetic acid emissions by displacing the acid-base
659 equilibrium towards the acid form (its conjugate base being acetate) and subsequently promoting
660 the aqueous-to-gaseous transfer by Henry equilibrium (Gabriel et al., 1999). Hill et al. (2002)
661 found a decrease in apoplastic pH with increasing leaf age (old leaves have a lower apoplastic pH
662 than young leaves). Thus, the increase in acetic acid emissions during senescence may have

resulted from a combination of a decrease of apoplast pH in senescent wheat leaves and the Maillard reaction.

4.3. Acetic acid and methanol uptake during wheat development

Acetic acid uptake from other cereal species (Bachy et al., 2016; Kesselmeier et al., 1998) and wheat (Bachy, 2018; Gonzaga Gomez et al., 2019) has been reported before and is well in line with our results during *Ripening*. As already discussed, acetic acid exchanges result from both, gas-to-liquid Henry equilibrium and acid-base equilibrium in the apoplast, as well as on any wet surface. As a result, acetic acid can either be emitted or taken up by plants depending on the concentration gradient between the plant and the atmosphere. If acetic acid concentration in the atmosphere is larger than in the plant it is deposited. During plant development, acetate and acetic acid may be converted to acetyl-CoA in the symplast and enter the plant metabolism, such as Krebs cycle (TCA, TriCarboxylic Acids cycle) (Seco et al., 2007). Thus this process allows maintaining a concentration gradient and, consequently, the continuous uptake of acetic acid by the living plant. This process ends with senescence, which may explain the switch from bidirectional acetic acid exchange to emission during that stage. Acetic acid deposition to wet surfaces in the chamber does not seem to be a dominant process. Otherwise, we would have expected some deposition after the rainfall events of 27 and 30 June, which was the case for acetone and methanol. On the contrary, acetic acid deposition was clear in Sen2 when no rainfall was observed (Figure 4).

Methanol uptake observed after harvest in this study may have resulted from its deposition and dissolution on wet surfaces following rainfall events. Indeed, methanol which is soluble in water can be taken up on water films that appear on the plant parts under wet conditions such as reported before (Bachy, 2018; Holzinger et al., 2001; Laffineur et al., 2012; Wohlfahrt et al.,

686 2015). In addition, after harvest the amount of biomass in the cuvette was small, presenting no
687 significant methanol emission to compensate deposition.

688 **4.4. *m/z* 73.064 emission during harvest**

689 The *m/z* 73.064 ion may correspond to methyl ethyl ketone (MEK). It has been suggested that
690 MEK emissions from plants may come from reduction reactions of isoprene oxidation products
691 produced during oxidative stress (Cappellin et al., 2019). In this study the ion *m/z* 73.064 showed
692 a gradual increase in emission rates during the senescence stages and a noticeable peak in
693 emissions two days after cutting wheat plants (Figure 4). A possible explanation is the reduction
694 reaction of isoprene-hydroxy-hydroperoxides (ISOPOOH, an isoprene oxidation product) to
695 MVK and then to MEK by an enzyme, alkenal-one oxidoreductase (AOR), that is ubiquitous in
696 terrestrial plants (Canaval et al., 2020). These authors have shown that this MEK formation
697 process responds to stomatal opening in leaving plants. During senescence and after harvest the
698 AOR enzyme may be more accessible to the ambient air, because of cells breakdown during
699 senescence, therefore leading to the observed increase in MEK emissions at the senescence stage.
700 Moreover, the same study reports that AOR is present in stem flows (xylem and phloem), which
701 would explain the burst observed after harvest. This would be consistent with the observation of
702 much larger MEK than MVK fluxes at all stages. Unfortunately, ISOPOOH could not be
703 measured with our PTR-TOF-MS, as it requires a specific setup of the drift tube to minimize
704 metal-catalysed decomposition of ISOPOOH Canaval et al. (2020).

705 In addition, a significant difference in MEK emissions is observed between the two plants after
706 harvest. This is also observed for other compounds including isoprene. Since these plants belong
707 to the same variety, a possible explanation for these differences in emissions between the two
708 wheat plants may be an important soil spatial heterogeneity of the field and therefore a different

availability of nutrients, water and also light for each plant. These different conditions may result, for each plant, in a more or less important production of isoprene as well as of the AOR enzyme responsible for the reduction of ISOPOOH to MEK.

4.5. Terpenes exchanges

Isoprene emissions increased gradually as senescence started (*Sen1*) and decreased when wheat plants entered chlorosis (*Sen2*) (Figure 4). However, when considering emissions in standard conditions (SEF) an additional increase is found during chlorosis (*Sen2*) (Figure 5). Isoprene increase with plant senescence has been reported before for wheat (Bachy, 2018) and maize (Mozaffar et al., 2018).

Much smaller, but still significant, emissions were measured for the *m/z* 137.133 compounds (potentially monoterpenes), generally an order of magnitude lower than isoprene emissions. A clear significant decrease in standard emission factors is noticed when plants entered senescence (Figure 5). This is consistent with literature where these compounds were found to present higher emissions during the early developmental stages of leaves and reduced emissions upon maturity and senescence for several plant species (Bracho-Nunez et al., 2011; Holopainen et al., 2010; Mozaffar et al., 2018). This relation between monoterpene emissions and plant development has been related to the antimicrobial or antifungal properties of these compounds and their great importance in young leaves which are more susceptible to herbivores and pathogen attacks than mature leaves (McCall and Fordyce, 2010). However, in the study of Bachy (2018) at the ecosystem level, monoterpenes emissions increased when wheat plants entered senescence. Monoterpenes emissions from soils have been reported before (Abis et al., 2018; Hayward et al., 2001). Thus, the increase in monoterpenes emissions found in Bachy (2018) may have resulted from soil emissions, which might explain the contradiction with our results.

4.6. *m/z* 108.957 and 125.959: compounds decreasing emissions with wheat senescence

Both *m/z* 108.957 and 125.959 compounds presented the same flux temporal trend with emission rates decreasing gradually as plants entered senescence and reaching minimum values from the second senescence period onwards (Figure 4). These ions may correspond respectively to nitrogen compounds with the chemical formula NO_4P^+ and $NO_5P.H^+$. However, since this is not a sure identification but rather some candidates that correspond very precisely to the mass, they may actually correspond to a single compound since they are quite well correlated to each other. To our knowledge, this is the first time these compounds are being reported in the literature regarding studies on BVOC emissions from crops. It is unlikely that they are chamber contaminants since they were not emitted by the empty chamber itself. In addition, if they were coming only from the chamber, they would remain stable throughout the experiment, while a clear daytime cycle is observed as well as a decrease during senescence.

4.7. GLV exchanges during wheat development

In earlier studies "green leaf volatiles" (GLV) compounds appeared to dominate BVOC emissions from wheat plants (Butter et al., 1985; König et al., 1995; Piesik et al., 2011). The ions *m/z* 99.079 and 101.092 were also detected in this study, and might represent hexenal and hexenol compounds, respectively, which are part of the GLV. In contrast with earlier studies, these compounds do not appear among the most emitted compounds in this study (Figure 3). Hexadiene (m/z 83.084) may also be a fragment of hexenol which shows larger concentrations than hexenol itself (Pang, 2015). Assuming m/z 83.084 is a fragment of hexenol, GLV fluxes become much larger and in better agreement with the literature. GLV compounds have antibiotic properties and inhibit the invasion of bacteria and other microorganisms into damaged tissues (Croft et al., 1993). This is why they are known to be released from plants following mechanical

755 tissue damage (Fall et al., 1999). Thus, in previous studies plants may have suffered further tissue
756 damage, which could explain the larger emissions of these compounds.

757 According to our results, the average emissions of these compounds seem to increase with onset
758 of senescence, which is well in line with literature findings. GLV production is known to
759 originate from the oxidation of fatty acids, catalyzed by 13-lipoxygenase (13-LOX) (Dudareva et
760 al., 2013). Fall et al. (1999) found an increase in emissions of (Z)-3-hexenal as detached aspen
761 leaves dried out. The authors proposed that during leaf drying, cellular water levels declined until
762 cellular structures began to collapse. This collapse was likely to induce the formation of hexenal
763 and hexanal compounds by increasing the oxidation of fatty acids, such as a-linolenic acid, which
764 may be released from membrane lipids. Holopainen et al. (2010) reported GLV dominating
765 BVOC emissions during the later stages of senescence and leaf abscission of *Betula pendula*
766 Roth, and suggested that the disintegration of cellular organelles and dying cells were related to
767 these emissions. Mozaffar et al. (2018) also showed increased hexenal emissions during maize
768 leaf senescence, and suggested that it could result from an increase in fatty acid oxidation in order
769 to provide energy for the senescence process.

770 **4.8. Robustness of the inferred standard emission factors**

771 The comparison between SEF-based whole plant VOC emissions and COV3ER-2016 whole
772 ecosystem fluxes allows us to challenge the robustness of the SEF estimated in this study and
773 especially their evolution over the plant developmental stages. This comparison allows evaluating
774 the representativeness of the measurements made with the two chambers and the intra-specific
775 variability of the VOCs emissions, and also evaluating the variation of the VOCs emissions
776 during the investigated development stages of wheat. However, the eddy covariance method,
777 unlike the plant chamber measurements, takes into account not only plant VOCs exchange but

778 also soil exchange. In addition, we should bear in mind that different wheat varieties between the
779 two studies might explain some observed differences in VOCs emissions.

780 For methanol, the larger SEF-based whole plant VOC emissions (representative of the whole
781 plant emissions) compared to the whole ecosystem fluxes may be explained by a significant sink
782 at the ground surface, due for instance to methanol dissolution in soil water. Indeed, the
783 contribution of soil to methanol uptake, under wet or dew conditions often present at night, is
784 well documented in the literature (Bachy et al., 2016; Holzinger et al., 2001; Karl et al., 2004). In
785 COV3ER-2016, the soil water content at 10 cm was around 30% humidity in volume, which is
786 quite wet. The canopy wetness as measured by the wetness sensor indicated that around 20% of
787 the day the canopy was wet. Overall, ripening was the wettest period.

788 Regarding acetic acid emissions, the SEF-based whole plant emissions did not match the EC
789 fluxes. Similarly to methanol, this is most likely due to the strong contribution of the soil to acetic
790 acid uptake, which was probably high enough to dominate the exchange of this compound and
791 overlook plant emissions during senescence. Indeed, Bachy et al. (2016) showed that the soil was
792 an important sink for acetic acid.

793 For all compounds, the observed differences between SEF-based whole plant emissions and EC
794 fluxes, especially large during *Sen2*, may also be explained by the temperature gradient in the
795 canopy and source location. Indeed, if the air temperature is replaced by the soil temperature in
796 the SEF model to mimic emissions by the bottom of the canopy, the modelled fluxes of methanol,
797 acetaldehyde and acetone fit much better to the measured ones during the senescence 2 phase
798 (Appendix F, Figure F.3 and Table F.1). This may be an indication of *Sen2* emissions rather
799 coming from the bottom leaves that are decomposing the most. In the chamber measurements,
800 these leaves were exposed to the same temperature as the entire plant due to efficient mixing in

801 the plant cuvette, which is not the case for the whole canopy that exhibits a large temperature
802 gradient between the cooler ground and the hotter top of the canopy. Moreover, this temperature
803 gradient is likely to increase with senescence due to vanishing transpiration leading to a lower
804 capacity to dissipate solar radiation into evaporation.

805 Comparison of the SEF and γ_{age} estimated in this study, in COV3ER2016, in Bachy et al. (2020)
806 and in Guenther et al. (2012), shows high similarities in SEF between this study and Guenther et
807 al. for methanol and acetone, but lower SEF and higher γ_{age} for acetaldehyde in this study
808 compared to Guenther (Table 3). One the contrary, COV3ER2016 compares very well with
809 Bachy et al. (2012), both in terms of SEF and γ_{age} for methanol and acetaldehyde. For
810 acetaldehyde this study COV3ER-2016 and Bachy et al. all agree well in terms of SEF and $\boldsymbol{\gamma_{age}}$,
811 while acetone emissions are larger in COV3ER2016 than in the three other datasets, and $\boldsymbol{\gamma_{age}}$ is
812 lower than 1 in COV3ER-2016.

813 This comparison suggests that methanol emissions by chamber measurements give larger
814 emissions (by a factor of ~3 to ~4) compared to whole ecosystem fluxes, probably due to soil and
815 plant recapture which would correspond to a large fraction of the emissions. Moreover, the effect
816 of senescence on methanol emissions is negligible in chamber measurements but large and
817 consistent at the canopy scale (factor of 3). The reason is still unclear but may be linked to
818 increased soil emissions (or decreased soil and plant recapture) during senescence.

819 **Table 3. Standard emission factors (SEF) and γ_{age} compared to existing dataset for wheat. G2012 stands for**
820 **Guenther et al. (2012), B2020 for Bachy et al. (2020) and COV3ER-2016 for Loubet et al. (2021).**

	Standard emisssion factor $\mu g\ m^{-2}\ h^{-1}$					γ_{age} -				
	This study	COV3ER-2016		G2012	B2020	This study	COV3ER-2016		G2012	B2020
Compound		Ta	Tsoil				Ta	Tsoil		
methanol	914	235	306	900	252	1.01	2.4	3.0	1.02	2.7
acetaldehyde	18	18	23	80	19	6.90	6.4	8.1	1.00	5.6
acetone	85	106	152	80	15	1.30	0.6	0.7	1.00	-

821

822 For acetaldehyde, whole plant emissions and whole ecosystem emissions are very similar and a
823 quarter of what is used in Megan 2.1 for crops. Senescence consistently induced an increase in
824 acetaldehyde emissions by a factor of 6 to 8 depending on the study, while Megan 2.1 did not
825 attribute any aging effect on acetaldehyde emissions. This consistently suggests a revision of the
826 emission factors and aging effects for acetaldehyde. For acetone, this study suggests Megan 2.1
827 SEF are valid, while the aging factor is unclear and diverges between studies.

828 Overall, this comparison suggests a real effect of senescence on the exchange of VOCs from
829 wheat plants leading to a clear increase in the emissions of acetaldehyde during this
830 developmental stage, and for methanol but at the ecosystem scale only. It also indicates that the
831 VOC fluxes measured on the two wheat plants in this study are well representative.

832 ## 5. Conclusions

833 In this study, BVOC exchanges from wheat plants were investigated from ripening to senescence
834 and after harvest, using 2 dynamic chambers, which constitutes a low number of replicates. With
835 regard to the emissions composition during the different investigated periods, methanol was the
836 most emitted compound (49 – 59% of the overall flux) followed by acetone, during ripening and
837 beginning of senescence (7.5 – 8.2% of the overall flux), and acetaldehyde, during the chlorosis

838 phase of senescence (9.7 of the overall flux). We showed that the composition of BVOC
839 emissions varied with wheat plant development. We noticed an increase in the contribution of
840 acetaldehyde and acetic acid to the overall emissions as senescence progressed (from 1.6 to 9.7%
841 and from 1.9 to 7.3% of the overall flux, respectively). We also demonstrated that the amounts of
842 BVOC exchanges varied significantly from one development period to another. The overall
843 BVOC emissions appeared to be twice as large during senescence compared to ripening. In
844 general, once normalized for temperature and light conditions, emissions of the major compounds
845 increased as senescence progressed. After harvest, BVOCs were emitted in small (3 times less
846 than during the ripening on average) but significant amounts, most likely from wheat stems. This
847 suggests that after harvest, the wheat stems left in the field may be a non-negligible source of
848 BVOC. OH reactivity of the emitted BVOC was calculated and showed a small reactivity on
849 average compared to measurements in isoprene or monoterpenes emitter canopies. The OH
850 reactivity however showed a peak of 12 s^{-1} during the first stage of senescence and a significant
851 contribution after harvest. Overall, senescence induced a marked increase in OH reactivity of up
852 to 4-fold during senescence 1 and 2-fold during senescence 2 compared to the ripening period.

853 Our measurements lasted only 4 days after the harvest. In order to consolidate our results, it may
854 be important to reproduce these measurements under similar conditions (soil, climate, agricultural
855 practices) on the same species but using more measuring chambers to enable statistical analyses.
856 Moreover, since the impact on atmospheric chemistry is highly dependent on the species of
857 compounds emitted, a good characterization of the emissions, including low emitting compounds,
858 is necessary. It would therefore be very useful to use GC-MS or a fast-GC in conjunction with
859 PTR-MS BVOC flux measurements in order to carry out an accurate identification of the

compounds. This would allow to better attribute fragments in particular of acetic acid at m/z 43 and green leaves volatiles at m/z 83.

BVOC emissions, and in particular oxygenated compounds, varied in composition and amounts with the development of wheat. This suggests that the current practice of assigning standard emission factors (SEF) by default to the entire plant season without considering larger emissions during plant senescence, may lead to an underestimation of BVOC emissions by wheat plants and possibly other crop species.

Comparison between whole plant emissions and ecosystem scale emissions suggests that methanol recapture in the canopy may represent a large fraction of the plant emitted methanol, while acetaldehyde emitted at the plant and ecosystem scales are comparable between the two approaches. It also clearly demonstrates a 5-to-8-fold increase of acetaldehyde emissions during senescence.

Acknowledgements

This study was supported by the region Île-de-France (DIM R2DS, Développement soutenable Réseau francilien de Recherche sur le Développement Soutenable, project n° 1656), ADEME (COV3ER, project n°1562C0032 and RAVISA, project n° 1762C0006) and the EU ICOS-RI Research Infrastructure. The PTR-Qi-ToF-MS is a national instrument supported by ANAEE-FR services (ANR project n°11-INBS-0001). SB acknowledges the European Union's Horizon 2020 research and innovation program (Marie-Sklodowska-Curie grant agreement n°674911-IMPACT). We gratefully thank Dominique Tristant and Yves Python from the AgroParisTech farm for giving access to the fields and sharing their information on practices, and Pascal Duprix

for helping building the chambers. Finally we thank Polina Voylokov for proofreading this manuscript.

Data access

Data are accessible in dataINRAE repository.

References

Abis, L., Loubet, B., Ciuraru, R., Lafouge, F., Dequiedt, S., Houot, S., Maron, P.A., Bourgeteau-Sadet, S., 2018. Profiles of volatile organic compound emissions from soils amended with organic waste products. Sci Total Environ 636, 1333–1343. https://doi.org/10.1016/j.scitotenv.2018.04.232

Baasandorj, M., Millet, D.B., Hu, L., Mitroo, D., Williams, B.J., 2015. Measuring acetic and formic acid by proton-transfer-reaction mass spectrometry: sensitivity, humidity dependence, and quantifying interferences. Atmospheric Measurement Techniques 8, 1303–1321. https://doi.org/10.5194/amt-8-1303-2015

Bachy, A., 2018. Echanges de composés organiques volatils d'origine biogénique entre deux écosystèmes agricoles et l'atmosphère. Université de Liège, Liège, Belgique.

Bachy, A., Aubinet, M., Amelynck, C., Schoon, N., Bodson, B., Delaplace, P., De Ligne, A., Digrado, A., du Jardin, P., Fauconnier, M.-L., 2020. Dynamics and mechanisms of volatile organic compound exchanges in a winter wheat field. Atmospheric Environment 221, 117105.

Bachy, A., Aubinet, M., Schoon, N., Amelynck, C., Bodson, B., Moureaux, C., Heinesch, B., 2016. Are BVOC exchanges in agricultural ecosystems overestimated? Insights from fluxes measured in a maize field over a whole growing season. Atmospheric Chemistry and Physics 16, 5343–5356. https://doi.org/10.5194/acp-16-5343-2016

Bracho-Nunez, A., Welter, S., Staudt, M., Kesselmeier, J., 2011. Plant-specific volatile organic compound emission rates from young and mature leaves of Mediterranean vegetation. Journal of Geophysical Research: Atmospheres 116. https://doi.org/10.1029/2010JD015521

Bsaibes, S., Gros, V., Truong, F., Boissard, C., Baisnée, D., Sarda-Esteve, R., Zannoni, N., Lafouge, F., Ciuraru, R., Buysse, P., Kammer, J., Gomez, L.G., Loubet, B., 2020. Characterization of Total OH Reactivity in a Rapeseed Field: Results from the COV3ER Experiment in April 2017. Atmosphere 11, 261. https://doi.org/10.3390/atmos11030261

Butter, R.G., Xu, C., Ling, L.C., 1985. Volatile components of wheat leaves (and stems): possible insect attractants. J. Agric. Food Chem. 33, 115–117. https://doi.org/10.1021/jf00061a033

Canaval, E., Millet, D., Zimmer, I., Nosenko, T., Georgii, E., Partoll, E., Fischer, L., Alwe, H., Kulmala, M., Karl, T., Schnitzler, J.-P., Hansel, A., 2020. Rapid conversion of isoprene photooxidation products in terrestrial plants 1, 44. https://doi.org/10.1038/s43247-020-00041-2

Cappellin, L., Loreto, F., Biasioli, F., Pastore, P., McKinney, K., 2019. A mechanism for biogenic production and emission of MEK from MVK decoupled from isoprene

biosynthesis. Atmospheric Chemistry and Physics 19, 3125–3135. https://doi.org/10.5194/acp-19-3125-2019

Christian, T., Kleiss, B., Yokelson, R., Holzinger, R., Crutzen, P., Hao, W., Shirai, T., Blake, D., 2004. Comprehensive laboratory measurements of biomass-burning emissions: 2. First intercomparison of open-path FTIR, PTR-MS, and GC-MS/FID/ECD. Journal of Geophysical Research-Atmospheres, v.109 (2004) 109. https://doi.org/10.1029/2003JD003874

Cojocariu, C., Kreuzwieser, J., Rennenberg, H., 2004. Correlation of short-chained carbonyls emitted from Picea abies with physiological and environmental parameters. New Phytologist 162, 717–727. https://doi.org/10.1111/j.1469-8137.2004.01061.x

Croft, KPC., Juttner, F., Slusarenko, A.J., 1993. Volatile Products of the Lipoxygenase Pathway Evolved from Phaseolus vulgaris (L.) Leaves Inoculated with Pseudomonas syringae pv phaseolicola. Plant Physiol 101, 13–24.

Das, M., Kang, D., Aneja, V.P., Lonneman, W., Cook, D.R., Wesely, M.L., 2003. Measurements of hydrocarbon air–surface exchange rates over maize. Atmospheric Environment 37, 2269–2277.

Dudareva, N., Klempien, A., Muhlemann, J.K., Kaplan, I., 2013. Biosynthesis, function and metabolic engineering of plant volatile organic compounds. New Phytol 198, 16–32. https://doi.org/10.1111/nph.12145

Fall, R., 2003. Abundant Oxygenates in the Atmosphere: A Biochemical Perspective. Chem. Rev. 103, 4941–4952. https://doi.org/10.1021/cr0206521

Fall, R., Benson, A.A., 1996. Leaf methanol — the simplest natural product from plants. Trends in Plant Science 1, 296–301. https://doi.org/10.1016/S1360-1385(96)88175-0

Fall, R., Karl, T., Hansel, A., Jordan, A., Lindinger, W., 1999. Volatile organic compounds emitted after leaf wounding: On-line analysis by proton-transfer-reaction mass spectrometry. Journal of Geophysical Research: Atmospheres 104, 15963–15974. https://doi.org/10.1029/1999JD900144

Fehsenfeld, F., Calvert, J., Fall, R., Goldan, P., Guenther, A.B., Hewitt, C.N., Lamb, B., Liu, S., Trainer, M., Westberg, H., Zimmerman, P., 1992. Emissions of volatile organic compounds from vegetation and the implications for atmospheric chemistry. Global Biogeochemical Cycles 6, 389–430. https://doi.org/10.1029/92GB02125

Feilberg, A., Liu, D., Adamsen, A.P.S., Hansen, M.J., Jonassen, K.E.N., 2010. Odorant emissions from intensive pig production measured by online proton-transfer-reaction mass spectrometry. Environ Sci Technol 44, 5894–5900. https://doi.org/10.1021/es100483s

Fukui, Y., Doskey, P.V., 2000. Identification of nonmethane organic compound emissions from grassland vegetation. Atmospheric Environment 34, 2947–2956. https://doi.org/10.1016/S1352-2310(00)00068-6

Gabriel, R., Schäfer, L., Gerlach, C., Rausch, T., Kesselmeier, J., 1999. Factors controlling the emissions of volatile organic acids from leaves of Quercus ilex L. (Holm oak). Atmospheric Environment 33, 1347–1355. https://doi.org/10.1016/S1352-2310(98)00369-0

Gallagher, M.W., Clayborough, R., Beswick, K.M., Hewitt, C.N., Owen, S., Moncrieff, J., Pilegaard, K., 2000. Assessment of a relaxed eddy accumulation for measurements of fluxes of biogenic volatile organic compounds: study over arable crops and a mature beech forest. Atmospheric Environment 34, 2887–2899. https://doi.org/10.1016/S1352-2310(00)00066-2

966 Gonzaga Gomez, L., Loubet, B., Lafouge, F., Ciuraru, R., Buysse, P., Durand, B., Gueudet, J.-C.,
967 Fanucci, O., Fortineau, A., Zurfluh, O., Decuq, C., Kammer, J., Duprix, P., Bsaibes, S.,
968 Truong, F., Gros, V., Boissard, C., 2019. Comparative study of biogenic volatile organic
969 compounds fluxes by wheat, maize and rapeseed with dynamic chambers over a short
970 period in northern France. Atmospheric Environment 214, 116855.
971 https://doi.org/10.1016/j.atmosenv.2019.116855
972 Gouinguené, S.P., Turlings, T.C.J., 2002. The effects of abiotic factors on induced volatile
973 emissions in corn plants. Plant Physiol. 129, 1296–1307.
974 https://doi.org/10.1104/pp.001941
975 Graus, M., Eller, A.S.D., Fall, R., Yuan, B., Qian, Y., Westra, P., de Gouw, J., Warneke, C.,
976 2013. Biosphere-atmosphere exchange of volatile organic compounds over C4 biofuel
977 crops. Atmospheric Environment 66, 161–168.
978 https://doi.org/10.1016/j.atmosenv.2011.12.042
979 Guenther, A., Hewitt, C.N., Erickson, D., Fall, R., Geron, C., Graedel, T., Harley, P., Klinger, L.,
980 Lerdau, M., Mckay, W.A., Pierce, T., Scholes, B., Steinbrecher, R., Tallamraju, R.,
981 Taylor, J., Zimmerman, P., 1995. A global model of natural volatile organic compound
982 emissions. J. Geophys. Res. 100, 8873–8892. https://doi.org/10.1029/94JD02950
983 Guenther, A.B., Jiang, X., Heald, C.L., Sakulyanontvittaya, T., Duhl, T., Emmons, L.K., Wang,
984 X., 2012. The Model of Emissions of Gases and Aerosols from Nature version 2.1
985 (MEGAN2.1): an extended and updated framework for modeling biogenic emissions.
986 Geoscientific Model Development 5, 1471–1492. https://doi.org/10.5194/gmd-5-1471-
987 2012
988 Hayward, S., Muncey, R.J., James, A.E., Halsall, C.J., Hewitt, C.N., 2001. Monoterpene
989 emissions from soil in a Sitka spruce forest. Atmospheric Environment 35, 4081–4087.
990 https://doi.org/10.1016/S1352-2310(01)00213-8
991 Hayward, S., Tani, A., Owen, S.M., Hewitt, C.N., 2004. Online analysis of volatile organic
992 compound emissions from Sitka spruce (Picea sitchensis). Tree Physiol. 24, 721–728.
993 https://doi.org/10.1093/treephys/24.7.721
994 Hill, P.W., Raven, J.A., Sutton, M.A., 2002. Leaf age-related differences in apoplastic NH4+
995 concentration, pH and the NH3 compensation point for a wild perennial. J Exp Bot 53,
996 277–286. https://doi.org/10.1093/jexbot/53.367.277
997 Holopainen, J.K., Heijari, J., Oksanen, E., Alessio, G.A., 2010. Leaf Volatile Emissions of Betula
998 pendula during Autumn Coloration and Leaf Fall. J Chem Ecol 36, 1068–1075.
999 https://doi.org/10.1007/s10886-010-9857-4
1000 Holzinger, R., Jordan, A., Hansel, A., Lindinger, W., 2001. Methanol measurements in the lower
1001 troposphere near Innsbruck (047 degrees 16'N; 011 degrees 24'E), Austria [WWW
1002 Document]. Atmospheric Environment. URL
1003 https://eurekamag.com/research/003/497/003497800.php (accessed 5.30.18).
1004 Isaksen, I.S.A., Granier, C., Myhre, G., Berntsen, T.K., Dalsoren, S.B., Gauss, M., Klimont, Z.,
1005 2009. Atmospheric composition change: Climate-chemistry interactions. Atmospheric
1006 Environment 43, 5138–5192. https://doi.org/Isaksen ISA, Granier C, Myhre G, Berntsen
1007 TK, Dalsoren SB, Gauss M, & Klimont Z <http://pure.iiasa.ac.at/view/iiasa/159.html>
1008 (2009). Atmospheric composition change: Climate-chemistry interactions. Atmospheric
1009 Environment 43 (33): 5138-5192. DOI:10.1016/j.atmosenv.2009.08.003
1010 <https://doi.org/10.1016/j.atmosenv.2009.08.003>.

1011 Jardine, K., Karl, T., Lerdau, M., Harley, P., Guenther, A., Mak, J.E., 2009. Carbon isotope
1012 analysis of acetaldehyde emitted from leaves following mechanical stress and anoxia.
1013 Plant Biol (Stuttg) 11, 591–597. https://doi.org/10.1111/j.1438-8677.2008.00155.x
1014 Kammer, J., Décuq, C., Baisnée, D., Ciuraru, R., Lafouge, F., Buysse, P., Bsaibes, S., Henderson,
1015 B., Cristescu, S.M., Benabdallah, R., Chandra, V., Durand, B., Fanucci, O., Petit, J.-E.,
1016 Truong, F., Bonnaire, N., Sarda-Estève, R., Gros, V., Loubet, B., 2019. Characterization
1017 of particulate and gaseous pollutants from a French dairy and sheep farm. Science of The
1018 Total Environment 135598. https://doi.org/10.1016/j.scitotenv.2019.135598
1019 Kari, E., Miettinen, P., Yli-Pirilä, P., Virtanen, A., Faiola, C.L., 2018. PTR-ToF-MS product ion
1020 distributions and humidity-dependence of biogenic volatile organic compounds.
1021 Karl, G.A., 2009. A new European plant-specific emission inventory of biogenic volatile organic
1022 compounds for use in atmospheric transport models. Biogeosciences 6.
1023 Karl, T., Guenther, A., Spirig, C., Hansel, A., Fall, R., 2003. Seasonal variation of biogenic VOC
1024 emissions above a mixed hardwood forest in northern Michigan. Geophysical Research
1025 Letters 30. https://doi.org/10.1029/2003GL018432
1026 Karl, T., Harren, F., Warneke, C., de Gouw, J., Grayless, C., Fall, R., 2005. Senescing grass crops
1027 as regional sources of reactive volatile organic compounds. J. Geophys. Res. 110,
1028 D15302. https://doi.org/10.1029/2005JD005777
1029 Karl, Thomas, Jobson, T., Kuster, W., Williams, E., Stutz, J., Shetter, R., Hall, S., Goldan, P.,
1030 Fehsenfeld, F., Lindinger, W., 2003. Use of proton-transfer-reaction mass spectrometry to
1031 characterize volatile organic compound sources at the La Porte super site during the Texas
1032 Air Quality Study 2000. Journal of Geophysical Research-Atmospheres 108.
1033 https://doi.org/10.1029/2002jd003333
1034 Kesselmeier, J., Bode, K., Gerlach, C., Jork, E.-M., 1998. Exchange of atmospheric formic and
1035 acetic acids with trees and crop plants under controlled chamber and purified air
1036 conditions. Atmospheric Environment 32, 1765–1775. https://doi.org/10.1016/S1352-
1037 2310(97)00465-2
1038 Kim, S., Guenther, A., Karl, T., Greenberg, J., 2011. Contributions of primary and secondary
1039 biogenic VOC tototal OH reactivity during the CABINEX (Community Atmosphere-
1040 Biosphere INteractions Experiments)-09 field campaign. Atmospheric Chemistry and
1041 Physics 11, 8613–8623. https://doi.org/10.5194/acp-11-8613-2011
1042 Kirstine, W., Galbally, I., Ye, Y., Hooper, M., 1998. Emissions of volatile organic compounds
1043 (primarily oxygenated species) from pasture. Journal of Geophysical Research:
1044 Atmospheres 103, 10605–10619. https://doi.org/10.1029/97JD03753
1045 König, G., Brunda, M., Puxbaum, H., Hewitt, C.N., Duckham, S.C., Rudolph, J., 1995. Relative
1046 contribution of oxygenated hydrocarbons to the total biogenic VOC emissions of selected
1047 mid-European agricultural and natural plant species. Atmospheric Environment 29, 861–
1048 874. https://doi.org/10.1016/1352-2310(95)00026-U
1049 Laffineur, Q., Aubinet, M., Schoon, N., Amelynck, C., Müller, J.-F., Dewulf, J., Langenhove,
1050 H.V., Steppe, K., Heinesch, B., 2012. Abiotic and biotic control of methanol exchanges in
1051 a temperate mixed forest. Atmospheric Chemistry and Physics 12, 577–590.
1052 https://doi.org/10.5194/acp-12-577-2012
1053 Laothawornkitkul, J., Taylor, J.E., Paul, N.D., Hewitt, C.N., 2009. Biogenic volatile organic
1054 compounds in the Earth system. New Phytologist 183, 27–51.
1055 https://doi.org/10.1111/j.1469-8137.2009.02859.x

Laufs, S., Cazaunau, M., Stella, P., Kurtenbach, R., Cellier, P., Mellouki, A., Loubet, B., Kleffmann, J., 2017. Diurnal fluxes of HONO above a crop rotation. Atmospheric Chemistry and Physics 17, 6907–6923. https://doi.org/10.5194/acp-17-6907-2017

Loreto, F., Centritto, M., Barta, C., Calfapietra, C., Fares, S., Monson, R.K., 2007. The relationship between isoprene emission rate and dark respiration rate in white poplar (Populus alba L.) leaves. Plant Cell Environ. 30, 662–669. https://doi.org/10.1111/j.1365-3040.2007.01648.x

Loubet, B., Buysse, P., Gonzaga-Gomez, L., Lafouge, F., Ciuraru, R., Decuq, C., Kammer, J., Bsaibes, S., Boissard, C., Durand, B., Gueudet, J.-C., Fanucci, O., Zurfluh, O., Abis, L., Zannoni, N., Truong, F., Baisnée, D., Sarda-Estève, R., Staudt, M., Gros, V., 2021. Volatile organic compound fluxes over a winter wheat field by PTR-Qi-TOF-MS and eddy covariance. Atmospheric Chemistry and Physics Discussions 1–38. https://doi.org/10.5194/acp-2020-1328

Loubet, B., Decuq, C., Personne, E., Massad, R.S., Flechard, C., Fanucci, O., Mascher, N., Gueudet, J.-C., Masson, S., Durand, B., Genermont, S., Fauvel, Y., Cellier, P., 2012. Investigating the stomatal, cuticular and soil ammonia fluxes over a growing tritical crop under high acidic loads. Biogeosciences 9, 1537–1552. https://doi.org/10.5194/bg-9-1537-2012

Loubet, B.B., Laville, P.P., Lehuger, S.S., Larmanou, E.E., Flechard, C.C., Mascher, N.N., Genermont, S.S., Roche, R.R., Ferrara, R.M.R.M., Stella, P.P., Personne, E.E., Durand, B.B., Decuq, C.C., Flura, D.D., Masson, S.S., Fanucci, O.O., Rampon, J.-N.J.-N., Siemens, J.J., Kindler, R.R., Gabrielle, B.B., Schrumpf, M.M., Cellier, P.P., 2011. Carbon, nitrogen and Greenhouse gases budgets over a four years crop rotation in northern France. Plant and Soil 343, 109–137. https://doi.org/10.1007/s11104-011-0751-9

McCall, A.C., Fordyce, J.A., 2010. Can optimal defence theory be used to predict the distribution of plant chemical defences? Journal of Ecology 98, 985–992. https://doi.org/10.1111/j.1365-2745.2010.01693.x

Morrison, E.C., Drewer, J., Heal, M.R., 2016. A comparison of isoprene and monoterpene emission rates from the perennial bioenergy crops short-rotation coppice willow and Miscanthus and the annual arable crops wheat and oilseed rape. GCB Bioenergy 8, 211–225. https://doi.org/10.1111/gcbb.12257

Mozaffar, A., Schoon, N., Bachy, A., Digrado, A., Heinesch, B., Aubinet, M., Fauconnier, M.-L., Delaplace, P., du Jardin, P., Amelynck, C., 2018. Biogenic volatile organic compound emissions from senescent maize leaves and a comparison with other leaf developmental stages. Atmospheric Environment 176, 71–81. https://doi.org/10.1016/j.atmosenv.2017.12.020

Niinemets, ü., Kuhn, U., Harley, P.C., Staudt, M., Arneth, A., Cescatti, A., Ciccioli, P., Copolovici, L., Geron, C., Guenther, A., Kesselmeier, J., Lerdau, M.T., Monson, R.K., Peñuelas, J., 2011. Estimations of isoprenoid emission capacity from enclosure studies: measurements, data processing, quality and standardized measurement protocols. Biogeosciences 8, 2209–2246. https://doi.org/10.5194/bg-8-2209-2011

Nölscher, A.C., Bourtsoukidis, E., Bonn, B., Kesselmeier, J., Lelieveld, J., Williams, J., 2013. Seasonal measurements of total OH reactivity emission rates from Norway spruce in 2011. Biogeosciences 10, 4241–4257. https://doi.org/10.5194/bg-10-4241-2013

Pang, X., 2015. Biogenic volatile organic compound analyses by PTR-TOF-MS: Calibration, humidity effect and reduced electric field dependency. J Environ Sci (China) 32, 196–206. https://doi.org/10.1016/j.jes.2015.01.013

Pape, L., Ammann, C., Nyfeler-Brunner, A., Spirig, C., Hens, K., Meixner, F.X., 2009. An automated dynamic chamber system for surface exchange measurement of non-reactive and reactive trace gases of grassland ecosystems. Biogeosciences 6, 405–429.

Piesik, D., Pańka, D., Delaney, K.J., Skoczek, A., Lamparski, R., Weaver, D.K., 2011. Cereal crop volatile organic compound induction after mechanical injury, beetle herbivory (Oulema spp.), or fungal infection (Fusarium spp.). Journal of Plant Physiology 168, 878–886. https://doi.org/10.1016/j.jplph.2010.11.010

Rottenberger, S., Kuhn, U., Wolf, A., Schebeske, G., Oliva, S.T., Tavares, T.M., Kesselmeier, J., 2005. Formaldehyde and acetaldehyde exchange during leaf development of the Amazonian deciduous tree species Hymenaea courbaril. Atmos. Environ. 39, 2275–2279. https://doi.org/10.1016/j.atmosenv.2004.12.027

Schade, G.W., Goldstein, A.H., 2001. Fluxes of oxygenated volatile organic compounds from a ponderosa pine plantation. Journal of Geophysical Research: Atmospheres 106, 3111–3123. https://doi.org/10.1029/2000JD900592

Seco, R., Peñuelas, J., Filella, I., 2007. Short-chain oxygenated VOCs: Emission and uptake by plants and atmospheric sources, sinks, and concentrations. Atmospheric Environment 41, 2477–2499. https://doi.org/10.1016/j.atmosenv.2006.11.029

Sindelarova, K., Granier, C., Bouarar, I., Guenther, A., Tilmes, S., Stavrakou, T., Müller, J.-F., Kuhn, U., Stefani, P., Knorr, W., 2014. Global data set of biogenic VOC emissions calculated by the MEGAN model over the last 30 years. Atmospheric Chemistry and Physics 14, 9317–9341. https://doi.org/10.5194/acp-14-9317-2014

Sinha, V., Williams, J., Crowley, J., J, L., 2008. The Comparative Reactivity Method—A new tool to measure total OH Reactivity in ambient air. Atmospheric Chemistry and Physics 8. https://doi.org/10.5194/acp-8-2213-2008

Staudt, M., Bertin, N., 1998. Light and temperature dependence of the emission of cyclic and acyclic monoterpenes from holm oak (Quercus ilex L.) leaves. Plant, Cell & Environment 21, 385–395. https://doi.org/10.1046/j.1365-3040.1998.00288.x

Steinbacher, M., 2004. Volatile organic compounds and their oxidation products in the atmospheric boundary layer: laboratory and field experiments (Doctoral Thesis). ETH Zurich. https://doi.org/10.3929/ethz-a-004751960

Sutton, M.A., Fowler, D., Burkhardt, J.K., Milford, C., 1995. Vegetation atmosphere exchange of ammonia: Canopy cycling and the impacts of elevated nitrogen inputs. Water Air Soil Pollut 85, 2057–2063. https://doi.org/10.1007/BF01186137

Taiz, L., Zeiger, E., Møller, I.M., Murphy, A., 2015. Plant physiology and development. Sunderland, MA: Sinauer Associates.

Tani, A., Hayward, S. and Hewitta, C.N., 2003. Measurement of monoterpenes and related compounds by proton transfer reaction-mass spectrometry (PTR-MS). International Journal of Mass Spectrometry, 223(1-3): 561-578.

Tani, A., Hayward, S., Hansel, A. and Hewitt, C.N., 2004. Effect of water vapour pressure on monoterpene measurements using proton transfer reaction-mass spectrometry (PTR-MS). International Journal of Mass Spectrometry, 239(2-3): 161-169. https://doi.org/10.1016/j.ijms.2004.07.020

Vlasenko, A., Macdonald, A.M., Sjostedt, S.J., Abbatt, J.P.D., 2010. Atmospheric Measurement Techniques Formaldehyde measurements by Proton transfer reaction – Mass.

Vuolo, R.M., Loubet, B., Mascher, N., Gueudet, J.-C., Durand, B., Laville, P., Zurfluh, O., Ciuraru, R., Stella, P., Trebs, I., 2017. Nitrogen oxides and ozone fluxes from an oilseed-

rape management cycle: the influence of cattle slurry application. Biogeosciences 14, 2225–2244. https://doi.org/10.5194/bg-14-2225-2017

Warneke, C., Karl, T., Judmaier, H., Hansel, A., Jordan, A., Lindinger, W., Crutzen, P.J., 1999. Acetone, methanol, and other partially oxidized volatile organic emissions from dead plant matter by abiological processes: Significance for atmospheric HOx chemistry. Global Biogeochemical Cycles 13, 9–17. https://doi.org/10.1029/98GB02428

Winer, A.M., Arey, J., Atkinson, R., Aschmann, S.M., Long, W.D., Morrison, C.L., Olszyk, D.M., 1992. Emission rates of organics from vegetation in California's Central Valley. Atmospheric Environment. Part A. General Topics 26, 2647–2659. https://doi.org/10.1016/0960-1686(92)90116-3

Wohlfahrt, G., Amelynck, C., Ammann, C., Arneth, A., Bamberger, I., Goldstein, A.H., Gu, L., Guenther, A., Hansel, A., Heinesch, B., Holst, T., Hörtnagl, L., Karl, T., Laffineur, Q., Neftel, A., McKinney, K., Munger, J.W., Pallardy, S.G., Schade, G.W., Seco, R., Schoon, N., 2015. An ecosystem-scale perspective of the net land methanol flux: synthesis of micrometeorological flux measurements. Atmospheric Chemistry and Physics 15, 7413–7427. https://doi.org/10.5194/acp-15-7413-2015

Ziemann, P.J., Atkinson, R., 2012. Kinetics, products, and mechanisms of secondary organic aerosol formation. Chem Soc Rev 41, 6582–6605. https://doi.org/10.1039/c2cs35122f

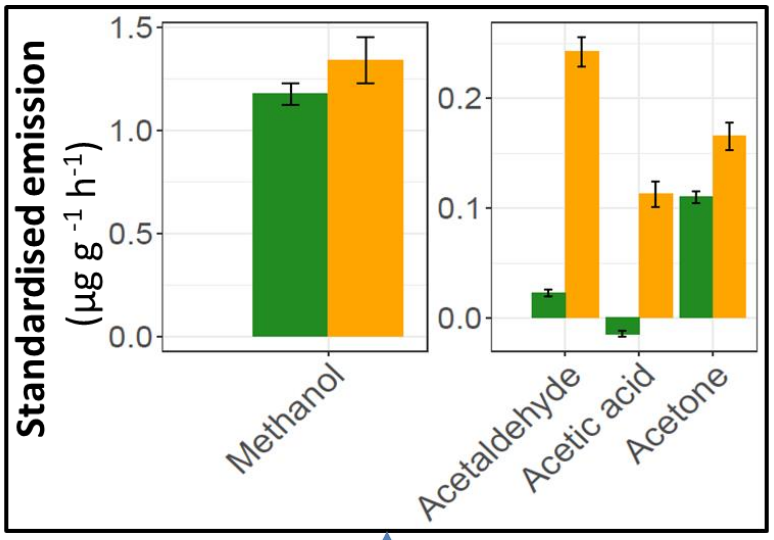

PTR-TOF-MS analysis

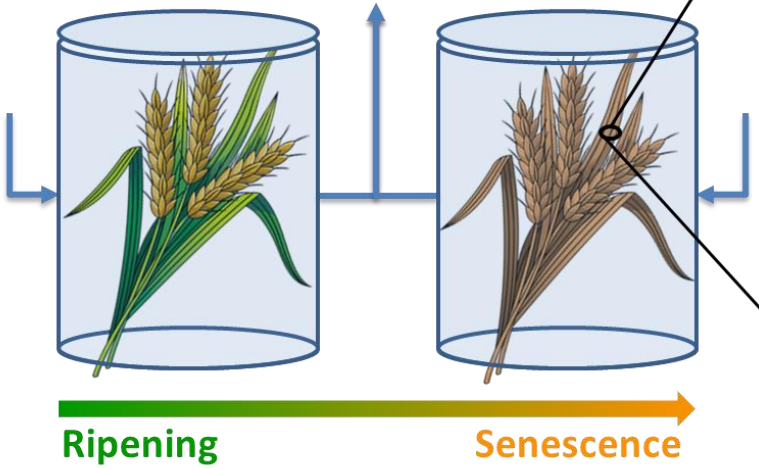

Hypothesized mechanisms